Publisher: Taylor & Francis & International Society of Limnology (SIL)

Journal: *Inland Waters*

DOI: 10.1080/20442041.2024.2327974

Bubble sizes inferred from bubble gas composition in a temperate freshwater fish pond

Carolin Waldemer[a,c], Michael Schwarz[b], Andreas Lorke[b], Bertram Boehrer[a], Matthias Koschorreck[a]

[a] Department of Lake Research, Helmholtz Centre for Environmental Research-UFZ, Germany

[b] Institute for Environmental Sciences, University of Kaiserslautern-Landau, Germany

[c] Corresponding author: Helmholtz Centre for Environmental Research-UFZ. E-mail address: carolin.waldemer@ufz.de

Abstract

Rising bubbles play a fundamental role in emitting greenhouse gases from shallow waters. Their size is crucial for bubble dissolution, gas exchange with the surrounding water, and the release of gases into the atmosphere. However, little is known about bubble sizes in shallow waters. To address this, we investigated bubble diameters in a 1.2 m deep fish pond, employing two methods: firstly, the bubble size distributions were measured by optical bubble sensors. Secondly, we used an existing single bubble dissolution model to determine diameters representative for the respective bubble size distributions at the water surface based on measured bubble oxygen contents and dissolved oxygen concentrations. Results from optical bubble sensors were relatively similar at all sites; however, subsequent analysis revealed problems particularly in detecting small bubbles under the turbid, shallow water conditions. Model-derived bubble diameters ranged from 0.5 to 10.5 mm, varied spatially within the pond, and displayed diurnal fluctuations. With increasing bubble flux, bubble diameters increased - bubbles at feeding sites were larger than in the open water area. A detailed sensitivity analysis revealed that, depending on the bubble size distribution, the uncertainty of the model increases with increasing water

depth. For a typical bubble diameter of 5 mm, the simple method can provide robust estimates of representative bubble size in waters shallower than 50 m.

Keywords: bubble size, bubble-sizer, ebullition, freshwater pond, model

1. Introduction

Ebullition, the gas flux via bubbles, is a very efficient transport pathway for climate-relevant gases like methane (CH_4) into the atmosphere (Bastviken et al., 2011). These fluxes are, however, difficult to determine and large uncertainties remain in current estimates of ebullitive greenhouse gas emissions (e.g., Rosentreter et al., 2021). In freshwater ecosystems, ebullition can account for > 80% of the total CH_4 emissions (e.g., Casper et al., 2000; DelSontro et al., 2010). Due to the high input of organic matter and shallow water depth, pond ecosystems, including artificial ponds in aquaculture, represent particular ebullition hotspots with high CH_4 emissions (Kosten et al., 2020; Rosentreter et al., 2021; Waldemer and Koschorreck, 2023; Zhang et al., 2022). While small bubbles may dissolve during their ascent through the water column, large bubbles dominate the gas transport (DelSontro et al., 2015; Greinert and Nützel, 2004; McGinnis et al., 2006; Ostrovsky et al., 2008). Especially in shallow waters, only a small fraction of the CH_4 initially contained in larger bubbles dissolves during bubble rise and can eventually be oxidised in the water (Delwiche and Hemond, 2017a; Kankaala et al., 2006). This underlines the importance of bubble sizes for determining the CH_4 flux into the atmosphere (DelSontro et al., 2015). So far, however, little is known about bubble sizes in freshwater ecosystems. To our knowledge, there is no published study investigating bubble sizes in ponds.

Bubbles form when the sum of the partial pressures of dissolved gases exceeds the sum of the atmospheric and hydrostatic pressure (Miyake, 1951). Nitrogen (N_2) and argon (Ar) enter water and sediment mainly via diffusion from the atmosphere and are usually represented in surface waters at gas pressures close to atmospheric partial pressure. As a consequence of its high water solubility, carbon dioxide (CO_2) usually contributes little to gas pressure. Only oxygen (O_2, in the water column by photosynthesis) and CH_4 (in the sediment by anaerobic decomposition of organic matter) are usually produced at rates high enough to raise gas pressure sufficiently for bubble formation (Boehrer et al., 2021). Since O_2 and CH_4 are produced or consumed by chemical and biological processes, their partial

pressures vary in dependence of the corresponding reaction rates (Boehrer et al., 2021; Madigan and Martinko, 2006). In equilibrium, the initial gas composition of bubbles reflects the ratio of partial pressures at the location of its formation (Boehrer et al., 2021). This is why, bubbles that leave reduced, methanogenic sediments consist mainly of CH_4 and N_2 in proportions that vary depending on CH_4 production and diffusive N_2 supply from the water column (Langenegger et al., 2019). During their ascent, they exchange gases with the surrounding water and lose CH_4 while taking up O_2 from the oxygenated water column (McGinnis et al., 2006). The rate of this gas exchange depends mainly on the surface to volume ratio of the bubbles and the time required to reach the surface. Water depth and initial bubble size are therefore important parameters, which determine if, and with what final gas composition, a bubble reaches the water surface and thus the atmosphere (Leifer and Patro, 2002).

Few studies have investigated the size spectrum of bubbles in freshwater ecosystems, but they suggest a rather narrow bubble size range with mean diameters of 4 to 6 mm and a high proportion of small bubbles (DelSontro et al., 2015; Delwiche and Hemond, 2017a; Ostrovsky, 2003; Ostrovsky et al., 2008). Measuring bubble sizes *in situ* is not trivial and methods are limited (e.g., Delwiche and Hemond, 2017a). There are two main approaches: acoustic and optical methods. Passive acoustic methods analyse the sound generated by oscillating bubbles upon their release from a solid surface using audio recordings (Leifer and Tang, 2006). The Minnart formula relates the sound frequency to the bubble size (Ivanova et al., 2022). More frequently, active acoustic methods are used: the rising bubbles are identified as individual acoustic targets in echograms and empirical relationships are used to convert acoustic backscatter strength to bubble volume (Ostrovsky et al., 2008). The latter can be used to survey large volumes of water (DelSontro et al., 2015), while acoustic shadows and external noise are the main limitations and complicate the analysis of dense bubble plumes, or the differentiation between organisms and bubbles (DelSontro et al., 2015; Ostrovsky et al., 2008). In addition, a minimum water depth is required to estimate the rise velocity, which is used to distinguish bubbles from other objects. Optical detection, the second major technology in use, can rely on image recognition algorithms that search for characteristic diffraction patterns or shapes (Al-Lashi et al., 2018). Bubble-sizers, on the other hand, use optical sensors to detect the passage of individual bubbles funnelled into a narrow transparent tube (Delwiche and Hemond, 2017a). They provide direct access

to bubble volume information and can be used in shallow waters. Here, the minimum water depth is determined by the design.

In this study, we tested an innovative method for determining representative bubble size at the water surface and the gas flux into the atmosphere by using the O_2 content of bubble gas collected with conventional bubble traps. We assumed that bubbles leaving the sediment were O_2-free (Avnimelech and Ritvo, 2003) and that the O_2 content at the water surface originated exclusively from stripping during the ascent. Hence bubble size is determined by water depth, dissolved O_2 concentrations and the bubble size (Leifer and Patro, 2002; McGinnis et al., 2006). Thus, a representative bubble size was calculated from the bubble O_2 content using an existing single bubble dissolution model (Greinert and McGinnis, 2009). For comparison, we measured bubble sizes with optical bubble-sizers according to the design of Delwiche and Hemond (2017a). The aim of this study was to apply and evaluate the described modelling approach, and to compare it with bubble-sizer measurements in a shallow freshwater fish pond. We hypothesized that bubble size is related to ebullition rates, leading to (1) spatially and temporally variable bubbles sizes and (2) increasing bubble sizes with increasing ebullition rate. To generalize our findings, we also estimated bubble sizes in ten adjacent, similarly managed fish ponds using data from Waldemer and Koschorreck (2023).

2. Methods

2.1 Study site description

Our study site, the 2.5 ha Gerstenteich fish pond, is 1.2 ± 0.3 m deep and located near Bautzen, Germany (51°29'N; 14°49'E; photos in Fig. S.1). According to the operator, the pond was constructed more than 400 years ago. After being drained in winter 2020/21, it was semi-intensively stocked with 580 kg ha^{-1} of catfish (Silurus glanis) and tench (Tinca tinca) in March 2021. A stationary pellet feeder dispensed a certain amount of fish food into the water below when triggered by fish. The automatic feeder was located at the harvest pit, which was the deepest point of the pond. Measures such as fertilisation, liming, aeration or dredging have not been taken. There was no significant in- or outflow of surface water but a high abundance of submerged water plants (in the center) and phytoplankton. Deciduous trees and reeds surrounded the eutrophic pond as a narrow belt of littoral vegetation

between adjacent grassland and farmland. As described in detail in Waldemer and Koschorreck (2023), ebullition decreased with radial distance from the feeding site (Fig. 1). Directly at the floating feeder (site S01), ebullition rates of 1238 mmol CH_4 m^{-2} d^{-1} and 177 mmol CO_2 m^{-2} d^{-1} were measured, which are the highest rates reported so far for natural and aquaculture systems (Waldemer and Koschorreck, 2023). Outside the zone influenced by the feeding site, CH_4 ebullition was 8 ± 7 mmol m^{-2} d^{-1} and the CO_2 content in the bubble gas was negligible. To generalize the findings at the Gerstenteich, data from ten adjacent, similarly managed fish ponds were included (Waldemer and Koschorreck, 2023). The two sites investigated in June 2021, one at the deeper, stationary feeding sites and one 55 m towards the pond center ("central sites"), are shown in Fig. 1.

2.2 Field work

Ebullition and bubble sizes were studied at the Gerstenteich in September 2021. Bubble traps were installed at the post of the pellet feeder (S01, water depth: 1.65 m) and at a distance of 42 m (S02, 1.20 m) and 83 m (S03, 1.15 m) to this in the direction of the pond center (to simplify, we distinguish between the "feeding site", S01 and immediate surroundings, and the "pond center", S02 and S03; Fig. 1). Gas samples were collected for two days every 3 h between 0530 h and midnight (2400 h) using a syringe and evacuated exetainers (Labco Limited, United Kingdom). If the gas volume was too small for complete gas analysis (≤ 3 mL), the sampling period was extended by another 3 h. Due to the high ebullition rate at S01, an additional 15th sampling was carried out there at midnight on the second day. During each sampling, vertical profiles of water temperature and dissolved O_2 were measured with a multiparameter probe (Sea & Sun Technologies, Germany) and water samples from approx. 15 cm depth were taken at S02 to determine dissolved CH_4 and CO_2 concentrations by headspace analysis. 30 mL of surface water and 30 mL of ambient air were shaken in a syringe for at least one minute. The headspace gas in the syringe was then transferred to an evacuated exetainer for later chromatographic analyses. In addition, water samples from the same depth were taken for chemical analysis like alkalinity which was measured by an automatic titrator (Metrohm) (details in Waldemer and Koschorreck, 2023). Near S02, dissolved O_2 was also logged every 6 s at around 35 cm water depth and at the bottom (RINKO I dissolved oxygen sensors, JFE Advantech Co., Ltd., Hyogo). Weather

data were monitored at the pellet feeder by a weather meter on a tripod (Kestrel 4500, Boothwyn, U.S.A.). At the ten adjacent ponds, the bubble gas was collected for 24 or 48 h, depending on the ebullition rate, and the gas composition was measured as described above. At the beginning and end of the sampling period, multiparameter probe profiles were taken.

To measure bubble size spectra directly, four optical bubble sensors according to the design of Delwiche and Hemond (2017a) were installed at the water surface on the first day between 1030 and 1100 h (Fig. 1). They automatically detected and recorded the number and sizes of bubbles collected by the attached inverted funnels until about noon on the third day. However, only the data coinciding with the application periods of the neighboring bubble traps were used. B01 and B02 were 7 and 5 m away from S01, while B03 and B04 were deployed around the middle of the transect about 17 m from S02 (distance from S01 44 and 70 m, from S03 60 and 44 m, respectively).

2.3 Gas analyses and calculations

The analysis of the total gas composition of the collected samples was achieved stepwise. For CH_4, N_2, and Ar, a gas chromatograph equipped with a 5% palladium catalyst (to remove O_2), a molecular sieve 13X column at 50°C, a flame ionization detector and a thermal conductivity detector were used with hydrogen as carrier gas (SRI-8610C, SRI instruments, Torrance, USA). CO_2 was analysed with a HaySep D column at 50°C, a flame ionization detector with methanizer and a thermal conductivity detector (N_2 as carrier gas). The calibration was adjusted to the concentration range of the samples. The injected volume depended on the sample volume. O_2 was measured directly in the sample vials using a needle-type optode (Firesting, Pyroscience, Aachen, Germany). As stated by the manufacturer, the accuracy of the O_2 sensor was about 1% of the measured concentrations with a detection limit of 0.02% O_2 (accuracy and resolution at 1% O_2: ± 0.02% and 0.01%; at 20% O_2: ± 0.2% and 0.05%). O_2 measurements were repeated every second to third sample to check the quality of the measurements. The sum of the analysed gases was 99 ± 2% (measurements deviating ≥ 5% from 100% were repeated, Table S.1).

Concentrations of dissolved CH_4 and CO_2 were calculated via eq. 1 from the gas concentrations in the equilibrated headspace of the samples using Henry's Law and temperature dependent solubility coefficients:

$$c_w = c_f \times \left(\frac{c_m\,(V_g + \beta \times V_w) - c_a V_g}{V_w}\right) \qquad with \qquad c_f = \frac{p}{R \times (T + 273.15)} \qquad \text{(eq. 1)}$$

c_w is the gas concentration in the water (µmol L^{-1}), c_m the measured volume-fraction (ppmv) and c_a the average atmospheric concentration (ppm). c_f is a conversion factor (mol L^{-1}) from mole fraction (ppm) to concentration (mmol m^{-3}) at *in situ* temperature (T in °C), *in situ* air pressure (p in kPa) and the molar gas constant R as 8.314 J K^{-1} mol^{-1}. V_g and V_w are the volumes of the headspace air and water sample used for equilibration (V_g and V_w in mL) and β is the Bunsen solubility calculated using temperature dependent solubility coefficients (dimensionless, Boehrer et al., 2021). We applied an alkalinity-based correction for CO_2 and the chemical equilibration of the carbonate system in the vials (Koschorreck et al., 2021).

2.4 Single bubble dissolution model

The single bubble dissolution model (SibuGUI) by Greinert and McGinnis (2009) describes gas transfer across the surface of an individual ascending bubble and tracks the dissolution and extraction of dissolved gases ("stripping" after McGinnis et al., 2006). It predicts changes in bubble size, gas composition and rise speed under a wide range of environmental conditions (Delwiche and Hemond, 2017b; Greinert and McGinnis, 2009). Based on an initial diameter and gas composition, the model calculates the bubble size and composition at the water surface as a function of water depth and dissolved gas concentrations (CH_4, CO_2 and O_2; N_2 in equilibrium with air). Further required inputs include water temperature, salinity and air pressure. Model assumptions and underlying equations are explained in detail in McGinnis et al. (2006).

We used version 1.2.6 of the SiBuGUI model to determine a bubble diameter representative for the bubble size distribution at the water surface based on precisely measured O_2 content in the bubble gas collected at the water surface. Assuming an O_2-free bubble formation in the sediment (Fig. S.2g, Avnimelech and Ritvo, 2003), the measured O_2 was stripped from the water column during bubble rise and provided information about the bubble size: as the bubble size decreases, the ratio of surface area

to volume and thus the gas exchange increases, and more O_2 is collected from the surrounding water in relation to the bubble volume (McGinnis et al., 2006). In addition, the bubble rise velocity, which is higher for large bubbles, determines the available time for gas exchange (e.g., McGinnis et al., 2006). Since dissolved O_2 in water was expected to change during the 3 h sampling periods, we calculated bubble sizes for the vertical dissolved O_2 profiles measured at the beginning and the end of each sampling period (Table S.1).

Since CH_4 and N_2 were the main components of bubbles originating from the sediment and their solubility and diffusion in water are very similar (Boehrer et al., 2021), we assumed pure CH_4 bubbles for our estimates. In a second step, we tested the effect of a complex bubble gas composition and used the measured gas composition to reconstruct the initial gas composition in the sediment. To test the effects of the O_2 concentration-dependent accuracy of the optode measurements on the model-derived bubble diameters, we determined the diameter deviations for the O_2 contents 0.5%, 1%, 5%, 10% and 17% (Table S.4). Normally distributed bubble size spectra were generated to test how the model-derived bubble diameters were related to the mean diameters of the distributions. For this, the distributions were divided into similar classes (number of classes, size of classes) and the model was applied to the mean bubble size of each class assuming pure CH_4 bubbles and the site conditions at S02 or a dissolved O_2 concentration of 100% saturation (Table S.5). Using the model-derived O_2 contents of these bubbles at the water surface, the O_2 fraction of the total gas volume at the water surface was estimated. Based on this, a model-derived bubble diameter was determined and compared with the mean value. In this way, the effects of varying bubble numbers, size distributions, dissolved O_2 concentrations, water depths, water temperatures and salinities were investigated. Since the model results were based on gas composition and volume, the Sauter mean diameter (SMD) was determined according to De Swart et al. (1996) to achieve better comparability:

$$SMD = (\sum_i D_i^3 \ / \ \sum D_i^2) \qquad \text{(eq. 2)}$$

with D_i denoting the diameters of individual bubbles under the assumption of a spherical shape. Similarly, the size distributions measured by the bubble-sizers were divided into 1 mm classes and used for comparison (Fig. S.5).

At the neighboring fish ponds, once a day, between 0830 and 2030 h at the different ponds, site-specific dissolved gas concentrations and water parameters were determined. For this reason, mean values of water temperature (23.6°C), salinity (0.19 PSU), and dissolved O_2 (4.9 mg L^{-1} or 51.0% at the feeding sites, 7.2 mg L^{-1} or 74.6% at the central sites) were fed into the model. Pure CH_4 bubbles were assumed to leave the sediment. Water depths varied between 0.5 and 2.5 m (Table S.6).

2.5 Bubble-sizers

Optical bubble-sizers were custom built after Delwiche and Hemond (2017a) with two modifications: a real time clock was added and the housing was downsized from two to one compartment. Individual bubbles that were funnelled into a 5 mm glass tube were detected by passing three photoelectric barriers (Fig. 1c). The first sensor detected the bubble and activated sensors two and three, which recorded the time of arrival and departure. Using the distance of 5 mm between sensors two and three, the length of the rising gas volume in the cylinder was calculated. Multiplication with the cross-sectional area of the glass tube provided the bubble volumes, which were used for calculating spherical diameters. Bubble passages that were detected consistently by all sensors were labelled as error-free. One or more out of seven error codes were assigned (details in Delwiche and Hemond, 2017a), if, e.g., not all sensors detected a bubble or it took more than 5 s to pass the sensor array ("erroneous detections"). The calibration was done according to Delwiche and Hemond (2017a) for bubble diameters of 1.6 to 22 mm. Bubbles with diameters much smaller than that of the glass tube failed to trigger detections because they did not diffract enough light while passing the photoelectric barriers. The upper size limit was set by the diameter and length of the glass tube, as the bubble volume needed to be smaller than the total volume of the tube. Moreover, the determination of the bubble volume relied on the constant bubble movement through the tube. For example, if large bubbles reached the upper end of the glass funnel while the bubble was still passing a sensor, this could have led to inconstant ascent speeds. Only error-free detected bubbles within the calibration range were used to determine the SMD (eq. 2) for each bubble trap sampling period. Ebullition rates were calculated based on the cumulative volume of all bubbles within the sampling periods assuming spherical bubbles.

To evaluate erroneous detections and potential measurement bias, laboratory experiments were performed in a glass column filled with tap water. The internal diameter of the glass tube of the bubble-sizer was 6 mm, compared to 5 mm in the field setup. Two main tests were performed: first, to test the effect of erroneous detections on estimated ebullition rates in clear water, constant bubbling was sampled for 3.5 h using a pump rate of 1 L h^{-1}. In a second experiment, two different syringe needles (internal diameter: 0.55 and 0.60 mm) were used to produce bubbles of different sizes. The size distributions were compared at different ebullition rates (0.4, 1.0, 2.0, 3.0 and 4.0 L h^{-1}).

2.6 Statistical analyses

R version 4.2.2 (R Core Team, 2022) and Origin 2022 (OriginLab Corporation, Northampton, MA, USA) software were used for statistical analysis and data visualisation. To test for significant differences and correlations, paired *t* tests and correlation matrices (Spearman's rank) were used. To analyse erroneous bubble-sizer detections for potential systematic bias, the data were grouped according to the assigned error codes including zero for no error. An ANOVA without the assumption of equal variance was calculated to determine if there were groups of errors with significantly different mean bubble diameters. Similarly, mean diameters from the bubble-sizers and the model were tested. In case of a significant difference and after checking for normality (Shapiro-Wilk test), Welch-tests for all combination of pairs were performed to test for differences between methods or data sets.

3. Results

3.1 O_2 modelling method

3.1.1 Model-derived bubble diameters

Dissolved O_2 concentrations varied diurnally between 14.7 and 2.5 mg L^{-1} in Gerstenteich and differed significantly ($P < 0.01$) between the feeding site and the pond center: mean dissolved O_2 was 5.6 ± 2.1 mg L^{-1} at S01 and 8.4 ± 1.7 mg L^{-1} at S02 and S03, where the dissolved O_2 concentration was higher by about 30 % saturation (Table 1 and S.2). In the morning around 0830 h when dissolved O_2 was lowest, the mean O_2 concentration of the profile was 28% saturation at S01, but was more than

twice as high at S02 and S03 (Fig. S.2, Table S.2). Dissolved O_2 at S01 varied over a wider range than at S02 and S03 (77% to 61 ± 4%) but had a similar diurnal pattern.

Bubble O_2 contents ranged from 0.5% to 11.9% (Fig. 2d, Table S.1) and were significantly ($P < 0.001$) lower at the feeding site: while only 0.9 ± 0.3% was measured at S01, mean bubble O_2 content was 5.9 ± 2.7% with diurnal variation at S02 and S03 (Table 1). The bubble gas at S01 contained 13 ± 3% CO_2, 79 ± 4% CH_4 and 7 ± 1% N_2, while in the pond center CO_2 was negligible (0.05 ± 0.10%) and CH_4 and N_2 accounted for 44 ± 7% and 48 ± 6%, respectively (Table S.1). Not only the bubble composition but also ebullition rates varied. Ebullition at the feeding site reached up to 56.5 L m^{-2} d^{-1} and was almost a factor 200 higher than at the central sites (Table 1). The stripping of dissolved O_2 by rising bubbles led to an O_2 ebullition of 14.6 mmol m^{-2} d^{-1} at S01, i.e. more than 30 times higher than at S02 and S03 (0.5 mmol m^{-2} d^{-1}). Assuming the latter for the entire Gerstenteich, the O_2 efflux was 0.4 kg d^{-1}.

Although CO_2 is highly water-soluble (Sander, 2015), the bubble gas in S01 contained significant amounts of CO_2, which influenced the bubble size. Considering the specific compositions instead of assuming pure CH_4 bubbles increased the bubble size at S01 by 0.4 ± 0.2 mm, while the change was negligible at S02 and S03 (0.01 ± 0.02 mm, Table S.1), confirming our initial approach. The simplification is therefore valid unless CO_2 is a major component of the gas composition at very high ebullition rates, when taking the specific gas composition into account leads to more accurate results. Reconstructed by the model, the initial gas composition was determined to 57.5 ± 11.9% CH_4, 39.0 ± 13.1% CO_2 and 3.6 ± 1.5% N_2 at S01 and 61.2 ± 7.8% CH_4 and 38.8 ± 7.8% N_2 at S02 and S03 (Table S.1).

As a consequence of varying dissolved O_2 concentrations and gas compositions, the model-derived bubble diameters were heterogeneous with 5 times larger bubbles at the feeding site: 7.2 ± 1.9 mm (4.2 to 10.5 mm) compared to 1.3 ± 0.6 mm at S02 and S03 (0.5 to 3.2 mm; Fig. 2a, Table 1 and S.1). The use of dissolved O_2 concentrations at the beginning and at the end of the respective sampling periods resulted in small deviations of 0.2 ± 0.3 mm at S02 and S03, but had a larger effect at S01, especially in the morning (1.5 ± 1.4 mm; Fig. 2a, Table S.1). In contrast to S02 and S03, S01 showed a

repeating diurnal pattern with smaller bubbles in the morning. As the bubble-sizers detected bubbles at a depth of approx. 35 cm (Fig. 1), we investigated the change in size during the bubble ascent from the bottom to the water surface at each site: the effect was small at S02 and S03 (0.02 ± 0.03 mm, relative change in volume: 4.8 ± 4.7%), but at S01, bubbles shrank by 0.5 ± 0.4 mm (20.7 ± 16.1%) during ascent through the 1.65 m water column. These changes correlated well with the initial CO_2 contents (R^2 of -0.95, $P < 0.001$).

To generalize our findings, we included data from ten similar fish ponds (Waldemer and Koschorreck, 2023). Measured O_2 bubble contents were consistently lower at the feeding sites despite the heterogeneity among the different ponds (1.4 ± 1.2% compared to 4.8 ± 4.3%). At the feeding sites, model-derived bubble diameters were twice as large as in the pond center confirming the pattern observed at the Gerstenteich: 4.2 ± 1.5 mm (1.1 to 6.6 mm) compared to 2.1 ± 1.6 mm (0.5 to 5.0 mm; Table S.6). Generally, bubble sizes increased with ebullition rates approaching a maximum diameter of 1 cm at extremely high rates (Fig. 3b). The pattern was consistent across the similar ponds.

3.2.2 Sensitivity analyses and examination of model results

To evaluate the dependency of the model-derived bubble diameters on input data variability, we performed sensitivity checks. The effect of the O_2 concentration-dependent accuracy of the optode sensor was checked in the O_2 range of our samples (0.5% to 17%). The error was 0.13 mm at an O_2 content of 1%, 0.02 mm at 5% O_2 and decreased further with increasing O_2 content, showing that the overall effects were small (Table S.4).

To check the representativeness of the model-derived bubble diameter, the deviation from the SMD was calculated for various hypothetical, normally distributed bubble size distributions (mean values: 2 to 8 mm, standard deviations: 0.5 to 2.6 mm, counts: 200 and 2000), dissolved O_2 concentrations (100% saturation, measured maximum and minimum concentrations at S02), water depths (1.2 to 50 m), temperatures (8 to 25°C) or salinities (0.17 to 10 PSU). For this, spherical CH_4 bubbles and Gerstenteich mean values of dissolved CO_2 and CH_4, water temperature and salinity were assumed (Table S.5). In the 25 cases compared, the deviations were small (0.07 ± 0.04 mm, 1.2 ± 0.8%) and relative errors of > 2% only occurred at depths ≥ 25 m. For a distribution of 2000 bubbles (mean:

4 mm, standard deviation: 1.3 mm) and water depths of 25 and 50 m, the deviations between the model-derived diameter and the SMD were 0.6 mm (12%) and 1.9 mm (51%), respectively. Since the O_2 content of small bubbles quickly equilibrated with the dissolved O_2 of the surrounding water, their information content for subsequent size determination was limited. With increasing water depth, this affected an increasing number of bubbles and the discrepancy between model-derived diameter and SMD increased. For a 1 mm bubble, most of the O_2 content change occurred within the first 5 m of ascent (Fig. S.3). For a 5 mm bubble, this occurred within 55 m. However, as water depth increases, also the proportion of small, equilibrated bubbles that dissolve during their ascent increases. Bubbles of 2.5 mm dissolve completely during a 50 m ascent. Therefore, the applicability of the method depends on both the bubble size distribution and the water depth.

In a next step, the measured bubble size distributions (Fig. S.5) were used to simulate the O_2 content of the bubble gas at the surface via the model (size distributions were divided into classes of 1 mm, mean bubble sizes of the classes and mean values of the water parameters measured at S01 and S02 were used as a basis for the model) in order to determine the model-derived bubble diameter of the respective distribution and compare it with the calculated SMD: the deviation between the model-derived diameter and SMD was only 0.1 ± 0.1 mm (relative error: 1.7 ± 2.3%). Using the spectrum of B04 with a number of large outlier bubbles (Fig. S.5 and S.6) and assuming a dissolved O_2 concentration of 100% saturation, the influence of water depth was further investigated. At water depths of 10 m, 25 m, and 50 m, deviations between the model-derived bubble diameter and SMD were only 0.7 mm (8%), 0.7 mm (8%), and 1.5 mm (13%), respectively. Simulations with a literature-based, typical bubble size of 5.3 mm (s. Table 2) and a dissolved O_2 concentration of 100% saturation showed that at a water depth of 50 m, the O_2 content of the bubble at the surface was 15.6% - still well below the equilibrated O_2 content of 21% if adjusted to the surrounding water. However, with significantly smaller bubble sizes such as in the center of the Gerstenteich (1.3 ± 0.6 mm), a bubble O_2 content of 17.0% is already reached after 5 m.

With mean model-derived bubble diameters and initial CH_4 concentrations, the CH_4 ebullition rate was estimated and compared to the measured CH_4 fluxes. The deviation was only 24 mmol m^{-2} d^{-1} at S01

(1.9%), -0.1 mmol m^{-2} d^{-1} at S02 (1.2%) and 0.3 mmol m^{-2} d^{-1} at S03 (10.2%), further confirming the representativeness of the model-derived bubble diameter.

3.2 Bubble-sizers

3.2.1 Bubble-sizer field measurements

The results of the bubble-sizer measurements were similar for all sites with a SMD of 6.3 ± 1.2 mm throughout the study period, which was in the range of the model-derived bubble diameters at S01 (Fig. 2a and b, Table 1 and S.7). Statistical analysis revealed significant differences between the model-derived diameters in the pond center and the SMD measured at B03 and B04. The determined ebullition rates were below 7000 mL m^{-2} d^{-1} and 130 mL m^{-2} d^{-1} at the feeding and central sites, respectively, and distinctly lower than those measured at S01 and S02 (Fig. 2c, Table 1). The unimodal size distributions showed a high proportion of smaller bubbles and, at B02 and B04, large outlier bubbles, which had a strong influence on the total gas volume (Fig. S.5 and S.6). Diurnal patterns did not emerge.

B01 and B02 at the feeding site had significantly more error-free bubble events (1710 and 1406) than B03 (117) and B04 (31), where ebullition was more sporadic and heterogeneous (Fig. S.4). However, the large number of bubble events at B01 and B02 led to data gaps. The reason is a technical aspect: to be energy efficient but have sufficiently fast sampling frequency, two modes of data storage are used. For fast recording, a small chip with limited memory is used whose content is uploaded to a SD card after a predefined period. The researcher has to make an educated guess regarding this period so that the temporary storage is not overflowing. The period cannot be too short since the download uses significant amounts of the battery life and no events can be detected during the data transfer. In addition, external noise in the form of e.g., aquatic insects can add recorded events leading to memory overflow. The available data at B01 und B02 (26% and 29% of the sampling intervals) is assumed to be representative for the respective sampling periods (Table S.7). Due to the lower ebullition rate at B03 and B04, we assumed that the entire time period has been recorded here. Moreover, for the first sampling periods, data is not available (Table S.7). This was probably due to thermal background

noise until the devices equilibrated with the water temperature and the readings from the photoelectric barrier in the infrared were stable.

B01 and B02 at the feeding site detected 78% and 73% of the recorded bubbles error-free, while in the pond center, only 63% and 57% were detected correctly (Table S.7 and Fig. S.7 a-d). Especially small bubbles < 2 mm and bubbles ≥ 13 mm were detected with errors (Fig. S.7 f and h). Error code 10 was the most frequent, meaning that detector two detected more bubbles than detector three, which can be caused by bubble coalescence in the glass tube, but also by zooplankton or floating debris (Delwiche and Hemond, 2017a). Similar reasons led to 11% excluded bubble events at B03 by a combination of different error codes. 34% (B01), 44% (B02), 56% (B03) and 62% (B04) of the bubbles detected erroneously had diameters that exceeded the mean diameter of the correctly detected bubbles.

3.2.2 Bubble-sizer laboratory experiments

To investigate potential artefacts, we performed laboratory experiments. To identify possible bias in the optical bubble size measurements, a data set was measured with a bubbling rate of 1 L h^{-1} over 3.5 h (Fig. S.8a-e). If errors were random, the histograms of erroneous and correctly detected bubbles would be similar. However, almost all bubbles < 4 mm were detected erroneously and also from 13 mm the erroneous detections seemed to increase again (Fig. S.8c and e). Likely, these bubbles were big enough to trigger detection but too small to move along a straight path through the glass funnel. However, despite small bubbles were more likely to be missed, only 1.6% of the gas volume of erroneously detected bubbles stemmed from bubbles < 4 mm (Fig. S.8e). In this experiment, about 1.4 L of bubble gas was detected correctly and about 0.328 L erroneously; 0.323 L were erroneously detected bubbles ≥ 4 mm.

In another test, bubbles were produced with two different syringe needles (internal diameter: 0.55 and 0.60 mm) at rates of 0.4, 1.0, 2.0, 3.0 and 4.0 L h^{-1}. As expected, a slight difference in bubble sizes was detected: for example, at a rate of 0.4 L h^{-1}, a mean value of 5.1 ± 0.7 mm was observed for the smaller syringe diameter compared to 5.9 ± 1.3 mm for the larger one (Fig. S.8f-j). In addition, at 4.0 L h^{-1}, a slight increase in size occurred, most likely due to increased coalescence of bubbles.

4. Discussion

Using measured bubble gas compositions in combination with an existing single bubble dissolution model (Greinert and McGinnis, 2009), we found significant spatial differences between bubble sizes at the feeding site and the center of a shallow fish pond, confirming our first hypothesis. At the feeding site at S01, the consistently low O_2 content of the bubble gas resulted in five times larger model-derived bubble diameters than at the center of the pond: 7.2 ± 1.9 mm compared to 1.3 ± 0.6 mm at S02 and S03 (Table 1). This pattern was confirmed by measurements in ten similar ponds: despite the heterogeneity found among the ponds, the consistently lower O_2 content in the bubble gas at the feeding sites resulted in larger bubble diameters here. Spatial heterogeneity of bubble sizes had been observed in previous studies (DelSontro et al., 2015; Delwiche and Hemond, 2017b; Ostrovsky, 2003), however not to this extent. The authors attributed this variability mainly to variations in ebullition rates and sediment properties: sediment properties, such as cohesiveness, affect bubble release and existing fractures might have served as conduits that allowed easier bubble transit (Algar et al., 2011; Algar and Boudreau, 2010; Scandella et al., 2011). Sediment characteristics did not differ significantly in the Gerstenteich (Waldemer and Koschorreck, 2023), however, as indicated by the measurements of Delwiche and Hemond (2017b), we found larger bubbles with increasing ebullition (Fig. 3b). Given that ebullition at the Gerstenteich feeding site was 38.7 ± 9.4 L m^{-2} d^{-1}, almost 200 times higher than in the center, spatial heterogeneity of the observed magnitude seems plausible. Furthermore, due to these high ebullition rates, the model-derived maximum bubble diameter of 10.5 mm at S01 may be considered a rough upper bubble size limit in these shallow ecosystems.

The bubble sizes measured with the optical bubble-sizers were relatively similar at all sites, with a SMD of 7.0 ± 3.2 mm, and differed significantly from the model-derived bubble diameters (Table 1). The measured bubble sizes are within the size ranges reported in other acoustic and optical studies in freshwater ecosystems (Table 2). In general, bubble size spectra measured with acoustic and optical methods tend to be relatively narrow with a high proportion of small bubbles (DelSontro et al., 2015; Delwiche and Hemond, 2017b; Greinert and Nützel, 2004; Hornafius et al., 1999; McGinnis et al., 2006; Ostrovsky, 2003; Ostrovsky et al., 2008; Vagle et al., 2010). However, these methods have

limitations, especially with respect to the detection of relatively small and large bubbles and the analysis of dense bubble plumes, which may coincide with large bubbles (DelSontro et al., 2015; Delwiche and Hemond, 2017a, 2017b; Ostrovsky et al., 2008). The locations of the bubble-sizers and the bubble traps were some meters apart, but the generally observed ebullition pattern (Waldemer and Koschorreck, 2023), the relationship between ebullition and bubble size in this and previous studies (Delwiche and Hemond, 2017b), and a comparison with additional sites to the left and right of the transect (Waldemer and Koschorreck, 2023) indicate that differences in bubble sizes at the feeding site and the pond center can be expected. In addition, the ebullition rates calculated from the bubble-sizer data were lower than the rates measured by the bubble traps. In the open water area, ebullition at B04 was about half the ebullition measured by eight bubble traps (Waldemer and Koschorreck, 2023).

In our measurements, bubble-sizers recorded a large proportion of erroneous bubble detections. While Delwiche and Hemond (2017a) detected 86% of bubbles error-free, the rate was lower (57% to 78%) under the turbid water conditions in the pond, where floating debris and aquatic organisms probably affected the optical detection. In addition, the high ebullition rates at the feeding site exceeded the data storage capacity of the system, resulting in data gaps. Our error analysis of the field and laboratory data indicated that especially small bubbles (< 2 and < 4 mm respectively; Fig. S.7f and S.8c and h) were detected with errors, which make up a large proportion of bubbles in natural bubble size distributions (e.g., DelSontro et al., 2015; Delwiche and Hemond, 2017b; Ostrovsky et al., 2008). This may explain the discrepancy in the determined bubble sizes in the pond center, where the size distributions were mainly composed of small bubbles. The error analysis at B03 and B04 indicated that also large bubbles were detected with errors, however, these errors could also have been caused by organisms and floating debris, which were visibly more abundant in the pond center. Since the model-derived diameters were four times smaller than the bubbles detected at B03 and B04, we assume that sporadically rising small bubbles possibly stuck to the outer funnel due to their lower buoyancy, and merged there before they detached and continued to rise through the detector. At the feeding sites, where larger bubbles dominated the size distributions, the deviation between model-derived and measured bubble sizes was relatively small (0.5 ± 0.4 mm). Our experiments indicated that the bubbles in this size range were detected similarly well (Fig S.8c), indicating that the deviation

may be due to the different locations and the decreasing ebullition rates with distance from the pellet feeder (Waldemer and Koschorreck, 2023). In summary, this means that the performance of the bubble-sizers depended on bubble size, with most reliable results for medium sized bubbles (from approx. 4 to 13 mm). It is thus possible that bubble sizes in freshwaters may be more variable than previously thought as especially small bubbles could have escaped the detection in former studies. This could possibly affect greenhouse gas emissions estimates made on the basis of bubble sizes. In the case of the Gerstenteich open water area, such estimates could have led to an overestimation of CH_4 ebullition.

These analyses and comparisons clearly support the results of the newly presented modelling method for estimating bubble size. It also provided insights into the initial gas composition of the bubbles leaving the sediment. At S01, the CH_4 ebullition rate was higher than any reported so far for natural and aquaculture systems (Waldemer and Koschorreck, 2023). Despite the high water solubility of CO_2 (Sander, 2015), anaerobic degradation also resulted in 177 mmol $m^{-2} d^{-1}$ CO_2 ebullition (Waldemer and Koschorreck, 2023). An initial CO_2 content of 39.0 ± 13.1% explained the measured rates and a N_2 content of only 3.6 ± 1.5% illustrated the effect of continuous gas stripping from the sediment pore water (Brennwald et al., 2005; McGinnis et al., 2006; Reeburgh, 1969). High CO_2 contents in biogas production show that these numbers were realistic: gas contents ranged between 50% and 70% CH_4 and 30% and 50% CO_2, depending on organic material and fermentation conditions (Weiland, 2010). The high initial CO_2 contents at S01 led to decreasing bubble sizes during the bubble ascent (0.5 ± 0.4 mm). Therefore, taking into account the measured bubble gas composition under these conditions led to more accurate model-derived bubble sizes. In contrast, ebullition in the pond center was within the known range for shallow, eutrophic ponds (Waldemer and Koschorreck, 2023). The contribution of CO_2 to the bubble gas composition was negligible, and the bubble sizes did not change much when the measured gas composition was considered instead of assuming pure CH_4 bubbles (0.01 ± 0.02 mm). This shows that under conditions commonly observed in natural freshwaters, in which CO_2 is not a significant component of the bubble gas (e.g., Boehrer et al., 2021), and ebullition rates are not particularly high, a complete analysis of the bubble gas composition is not necessary to determine the correct bubble size. It is sufficient to assume pure CH_4 bubbles.

Model-derived bubble sizes depend on dissolved O_2 concentrations in the water column. By using two profiles, one from the beginning and one from the end of the 3 h sampling periods, we determined a size range that accounted for changing dissolved O_2 concentrations. While differences were small at S02 and S03 (0.2 ± 0.3 mm), differences of up to 4.2 mm occurred at S01 in the morning (Table S.1). This was due to the low but rapidly increasing dissolved O_2 concentrations in the water column at S01. Due to the high respiratory O_2 demand and continuous bubbling, the mean concentration of dissolved O_2 was < 30% saturation at around 0830 h but reached 120% in the early afternoon (Fig. S.2). As the O_2 concentration increases, so does the concentration gradient that drives diffusive gas transfer into the bubble (McGinnis et al., 2006). That the strongly fluctuating O_2 contents of the water column were the reason for the deviations at the high ebullition site S01 was further demonstrated when the dissolved O_2 was averaged over the entire study period to compare the model-derived bubble diameters with the mean values of the 3 h sampling periods: the deviation at S02 and S03 was negligible (0.1 ± 0.1 mm), while the deviation at S01 was 1.5 mm. In addition, using the mean dissolved O_2 content of S02 for two additional bubble traps (Waldemer and Koschorreck, 2023; approx. 24 and 43 m from S02 and 19 and 27 m from B03 and B04), bubble diameters of 1.5 ± 0.9 mm were determined, comparable to those at S02 and S03. Besides confirming the order of magnitude of the bubble sizes determined at S02 and S03, these considerations show that within a fluctuation range of 125 to 60% saturation (mean value 92%) like at S02 and S03, an average O_2 concentration can be sufficient for estimating the bubble size.

Although the mean dissolved O_2 concentration was high in the afternoon, the bubble O_2 contents at S01 remained low throughout the day. This resulted in a diurnal pattern with larger bubble diameters during the day without correlating with increased ebullition rates. In contrast, at S02 and S03, the tendency towards higher bubble O_2 contents at times of higher dissolved O_2 concentrations resulted in rather constant bubble sizes. To date, diurnal variations in bubble size have not been investigated and this is the first study in which this has been observed (Table 2). The low bubble O_2 content at S01 can be attributed to extremely high ebullition rates and frequently observed bubble plumes at the site. A bubble plume-induced flux of O_2-depleted, near-bottom water could occur, in which the bubbles rise to the water surface (Leifer and Patro, 2002; McGinnis et al., 2004). The locally reduced O_2 levels

would reduce gas transfer into the bubbles. These plumes occur episodically and would not be recorded by the measurements of the multi-parameter probe and therefore would not be included in the model. Also, in bubble plumes, the rise velocity of the bubbles increases, further reducing gas exchange with the surrounding water (e.g., McGinnis et al., 2006). These processes could potentially lead to an overestimation of bubble size at S01, but they do not explain the repeated diurnal pattern. Since Waldemer and Koschorreck (2023) observed a tendency of higher ebullition rates in the morning, which could not be explained by physical parameters such as temperature or atmospheric pressure and were attributed to bioturbation, we can assume that the smaller bubbles are due to the increased activity of the benthivorous fish. Muddy sediments behave mechanically as a fracture-elastic solid, so gas migration is determined by a fracture-dominated regime due to the large capillary-entry pressure (Katsman et al., 2013; Sirhan et al., 2019). Sediment disturbance by fish could directly trigger the release of smaller bubbles, but could also reduce the counter pressure of the sediment and open additional conduits for the bubbles through sediment displacement (Algar and Boudreau, 2010; Johnson et al., 2002; Scandella et al., 2011). Since fish activity was highest at the feeding site, the diurnal variations in bubble size occurred here.

To determine the bubble size via the model, the bubble rising from anoxic sediments needs to have O_2 contents in a measurable range and below the equilibrium concentration. In the O_2 range of the bubble gas at S01, small changes in the O_2 content can lead to differences in the model-derived bubble diameters. However, the accuracy of the O_2 measurement caused only a small error (0.13 ± 0.03 mm). Potential O_2 contamination during sampling and analysis would result in smaller bubble diameters, however, bubble gas contents as low as 0.08% O_2 (water column ~50 cm, data not shown) indicate that such contamination may have occurred only to a limited extent. Such an O_2 contamination would reduce the model-derived bubble diameter by 0.4 ± 0.2 mm at S01, while at S02 and S03, the changes would be negligible (0.02 ± 0.01 mm; using the site-specific mean O_2 content of the bubble gas and the minimum and maximum dissolved O_2 concentrations measured).

When the ratio of surface area to volume is important, the Sauter mean diameter (SMD) is used to represent size distributions. Compared to the arithmetic mean, the influence of a relatively small

number of large bubbles can be better taken into account (De Swart et al., 1996). Greinert and Nützel (2004) reported that > 50% of the gas volume in their experiments came from the largest 7% of the bubbles, and DelSontro et al. (2015) found that the largest 10% of the bubbles were responsible for > 65% of the total CH_4 emission, illustrating that large bubbles transport disproportionately large amounts of CH_4 into the atmosphere. This is why, as in DelSontro et al. (2015), we calculated the SMD as the diameter of a spherical bubble that would have the same ratio of surface area to volume as the investigated size distributions. Using simulated normal and *in situ* measured bubble size distributions, only very small deviations were found between SMD and model-derived diameters (0.07 ± 0.04 mm, water depth < 25 m). Although large outlier bubbles had the potential to bias the model-derived diameters, the diameters corresponded well to the SMD. The applicability of the method is, however, limited by the water depth: the ponds studied were between 0.5 and 2.5 m deep, but in systems that are very shallow, it may not be possible to install a bubble trap. In addition, the discrepancies between model-derived bubble diameters and SMD increased at water depths of 25 m as, with increasing depth, more and more small bubbles equilibrate with the dissolved O_2 concentrations of the surrounding water and do not contain representative information on bubble size. However, at a water depth of 50 m, this discrepancy was still < 2 mm (normal and *in situ* measured bubble size distributions assuming a dissolved O_2 concentration of 100% saturation). Using a literature-based, typical bubble size of 5.3 mm (Table 2) and a water depth of 50 m, the model-derived bubble O_2 content was still well below the equilibrium O_2 content of 21%. Furthermore, the CH_4 ebullition derived from the model results and the measured CH_4 ebullition agreed well. The discrepancy was small, even at the feeding site (relative deviation: 2%). This shows that the model-derived bubble diameters were representative for both the bubble size distributions and the gas flux into the atmosphere.

Another aspect to which this study draws attention is the effect of O_2 stripping from the water column by rising bubbles. The observed O_2 ebullition was within the range reported in the literature (Koschorreck et al., 2017; Long et al., 2020). A net ecosystem production of 0.1 mg C L^{-1} d^{-1} was determined for the study period (Waldemer and Koschorreck, 2023), meaning that, with a mean water depth of 1.2 m, photosynthesis provided about 3.6 kg O_2 d^{-1}. Based on the data of S02 and S03, about

10.7% of this O_2 (0.4 kg d^{-1}) was lost to the atmosphere via O_2 ebullition. Due to the high ebullition, this efflux was more than 30 times higher at S01. This suggests that the lower dissolved O_2 concentrations were not only caused by respiration, but also by constant O_2 stripping. Therefore, depending on the ebullition rate, O_2 ebullition can have significant impacts on the O_2 budget in the water, even if bubble O_2 contents and dissolved O_2 concentrations are low.

All in all, the O_2 modelling method provided bubble sizes representative for the respective bubble size distributions at the water surface and enabled new insights into the bubble size range in shallow freshwater ponds. With increasing ebullition rates, the bubble sizes increased and the CH_4 ebullition estimated from the model results agreed well with the measured rates even at the feeding sites. Despite the concern that large outlier bubbles could limit the validity of the model-derived bubble diameters, the method proved to be a good and simple alternative to optical bubble-sizers. Depending on the bubble size distribution, the applicability is, however, limited by the water depth and the discrepancies between model-derived bubble diameters and SMD increased at water depths of 25 m. In addition, as the method is sensitive to dissolved O_2, a representative mean value or several measurements over the day are recommended. To determine the bubble size rising from anoxic sediments, the bubble needs to have an O_2 content in a measurable range and below the equilibrium concentration. Nevertheless, for shallow waters, where ebullition is a significant greenhouse gas pathway to the atmosphere and measurements of bubble sizes are difficult, the O_2 modelling method can provide a reliable method for estimating a representative bubble size.

Declaration of Competing Interest

The authors declare that they have no known competing financial interests or personal relationships that could have appeared to influence the work reported in this paper.

Data availability

Data is available in the extensive appendix. If further data is required, it will be provided upon request.

Acknowledgment

We thank Martin Wieprecht, Thomas Bechle, Hannah Mihm, and Patrick Aurich for their eminent help during field and laboratory work. In addition, we thank the fish companies, especially Teichwirtschaft Kauppa in 02694 Großdubrau the owner of the Gerstenteich, for their support and constructive cooperation. This research was financed by the German Research Foundation (DFG) (Grant numbers KO 1911/7-1 and LO 1150/16).

Appendix A. Supporting Information

Supplement data associated with this article can be found online at doi…

References

Algar, C.K., Boudreau, B.P., 2010. Stability of bubbles in a linear elastic medium: Implications for bubble growth in marine sediments. J. Geophys. Res. 115, F03012. https://doi.org/10.1029/2009JF001312

Algar, C.K., Boudreau, B.P., Barry, M.A., 2011. Release of multiple bubbles from cohesive sediments. Geophys. Res. Lett. 38. https://doi.org/10.1029/2011GL046870

Al-Lashi, R.S., Gunn, S.R., Webb, E.G., Czerski, H., 2018. A Novel High-Resolution Optical Instrument for Imaging Oceanic Bubbles. IEEE J. Ocean. Eng. 43, 72–82. https://doi.org/10.1109/JOE.2017.2660099

Avnimelech, Y., Ritvo, G., 2003. Shrimp and fish pond soils: processes and management. Aquaculture 220, 549–567. https://doi.org/10.1016/S0044-8486(02)00641-5

Bastviken, D., Tranvik, L.J., Downing, J.A., Crill, P.M., Enrich-Prast, A., 2011. Freshwater Methane Emissions Offset the Continental Carbon Sink. Science 331, 50–50. https://doi.org/10.1126/science.1196808

Boehrer, B., Jordan, S., Leng, P., Waldemer, C., Schwenk, C., Hupfer, M., Schultze, M., 2021. Water | Free Full-Text | Gas Pressure Dynamics in Small and Mid-Size Lakes [WWW Document]. URL https://www.mdpi.com/2073-4441/13/13/1824 (accessed 3.24.22).

Brennwald, M.S., Kipfer, R., Imboden, D.M., 2005. Release of gas bubbles from lake sediment traced by noble gas isotopes in the sediment pore water. Earth Planet. Sci. Lett. 235, 31–44. https://doi.org/10.1016/j.epsl.2005.03.004

Casper, P., Maberly, S.C., Hall, G.H., Finlay, B.J., 2000. Fluxes of methane and carbon dioxide from a small productive lake to the atmosphere. Biogeochemistry 49, 1–19. https://doi.org/10.1023/A:1006269900174

De Swart, J.W.A., van Vliet, R.E., Krishna, R., 1996. Size, structure and dynamics of "large" bubbles in a two-dimensional slurry bubble column. Chem. Eng. Sci. 51, 4619–4629. https://doi.org/10.1016/0009-2509(96)00265-5

DelSontro, T., McGinnis, D.F., Sobek, S., Ostrovsky, I., Wehrli, B., 2010. Extreme Methane Emissions from a Swiss Hydropower Reservoir: Contribution from Bubbling Sediments. Environ. Sci. Technol. 44, 2419–2425. https://doi.org/10.1021/es9031369

DelSontro, T., McGinnis, D.F., Wehrli, B., Ostrovsky, I., 2015. Size Does Matter: Importance of Large Bubbles and Small-Scale Hot Spots for Methane Transport. Environ. Sci. Technol. 49, 1268–1276. https://doi.org/10.1021/es5054286

Delwiche, K.B., Hemond, H.F., 2017a. An enhanced bubble size sensor for long-term ebullition studies. Limnol. Oceanogr. Methods 15, 821–835. https://doi.org/10.1002/lom3.10201

Delwiche, K.B., Hemond, H.F., 2017b. Methane Bubble Size Distributions, Flux, and Dissolution in a Freshwater Lake. Environ. Sci. Technol. 51, 13733–13739. https://doi.org/10.1021/acs.est.7b04243

Greinert, J., McGinnis, D.F., 2009. Single bubble dissolution model – The graphical user interface SiBu-GUI. Environ. Model. Softw. 24, 1012–1013. https://doi.org/10.1016/j.envsoft.2008.12.011

Greinert, J., Nützel, B., 2004. Hydroacoustic experiments to establish a method for the determination of methane bubble fluxes at cold seeps. Geo-Mar. Lett. 24, 75–85. https://doi.org/10.1007/s00367-003-0165-7

Hornafius, J.S., Quigley, D., Luyendyk, B.P., 1999. The world's most spectacular marine hydrocarbon seeps (Coal Oil Point, Santa Barbara Channel, California): Quantification of emissions. J. Geophys. Res. Oceans 104, 20703–20711. https://doi.org/10.1029/1999JC900148

Ivanova, I.N., Budnikov, A.A., Malakhova, T.V., Grishanina, N.A., Dyemin, I.D., 2022. Monitoring the Bubble Flux of a Shallow-Water Seep Using Passive Acoustics with Allowance for the Effect of the Type of Underlying Surface. Bull. Russ. Acad. Sci. Phys. 86, 190–193. https://doi.org/10.3103/S1062873822020113

Johnson, B.D., Boudreau, B.P., Gardiner, B.S., Maass, R., 2002. Mechanical response of sediments to bubble growth. Mar. Geol. 187, 347–363. https://doi.org/10.1016/S0025-3227(02)00383-3

Kankaala, P., Huotari, J., Peltomaa, E., Saloranta, T., Ojala, A., 2006. Methanotrophic activity in relation to methane efflux and total heterotrophic bacterial production in a stratified, humic, boreal lake. Limnol. Oceanogr. 51, 1195–1204. https://doi.org/10.4319/lo.2006.51.2.1195

Katsman, R., Ostrovsky, I., Makovsky, Y., 2013. Methane bubble growth in fine-grained muddy aquatic sediment: Insight from modeling. Earth Planet. Sci. Lett. 377–378, 336–346. https://doi.org/10.1016/j.epsl.2013.07.011

Koschorreck, M., Hentschel, I., Boehrer, B., 2017. Oxygen Ebullition From Lakes: Oxygen Ebullition From Lakes. Geophys. Res. Lett. 44, 9372–9378. https://doi.org/10.1002/2017GL074591

Kosten, S., Almeida, R.M., Barbosa, I., Mendonça, R., Santos Muzitano, I., Sobreira Oliveira-Junior, E., Vroom, R.J.E., Wang, H.-J., Barros, N., 2020. Better assessments of greenhouse gas emissions from global fish ponds needed to adequately evaluate aquaculture footprint. Sci. Total Environ. 748, 141247. https://doi.org/10.1016/j.scitotenv.2020.141247

Langenegger, T., Vachon, D., Donis, D., McGinnis, D.F., 2019. What the bubble knows: Lake methane dynamics revealed by sediment gas bubble composition. Limnol. Oceanogr. 64, 1526–1544. https://doi.org/10.1002/lno.11133

Leifer, I., Patro, R.K., 2002. The bubble mechanism for methane transport from the shallow sea bed to the surface: A review and sensitivity study. Cont. Shelf Res., Gas in Marine Sediments: Contributions from the 5th International Conference orgainsed by the Shallow Gas Group, Bologna, Italy, September 1998 22, 2409–2428. https://doi.org/10.1016/S0278-4343(02)00065-1

Leifer, I., Tang, D., 2006. The acoustic signature of marine seep bubbles. J. Acoust. Soc. Am. 121, EL35–EL40. https://doi.org/10.1121/1.2401227

Long, M.H., Sutherland, K., Wankel, S.D., Burdige, D.J., Zimmerman, R.C., 2020. Ebullition of oxygen from seagrasses under supersaturated conditions. Limnol. Oceanogr. 65, 314–324. https://doi.org/10.1002/lno.11299

Madigan, M.T., Martinko, J.M., 2006. Brock Mikrobiologie, 11th ed. Pearson Studium, München.

McGinnis, D.F., Greinert, J., Artemov, Y., Beaubien, S.E., Wüest, A., 2006. Fate of rising methane bubbles in stratified waters: How much methane reaches the atmosphere? - McGinnis - 2006 - Journal of Geophysical Research: Oceans - Wiley Online Library [WWW Document]. URL https://agupubs.onlinelibrary.wiley.com/doi/full/10.1029/2005JC003183 (accessed 3.24.22).

McGinnis, D.F., Lorke, A., Wüest, A., Stöckli, A., Little, J.C., 2004. Interaction between a bubble plume and the near field in a stratified lake: BUBBLE PLUME LAKE INTERACTION. Water Resour. Res. 40. https://doi.org/10.1029/2004WR003038

Miyake, Y., 1951. The Possibility and the Allowable Limit of Formation of Air Bubbles in the Sea [WWW Document]. URL https://www.jstage.jst.go.jp/article/mripapers1950/2/1/2_95/_article/-char/ja/ (accessed 3.24.22).

Ostrovsky, I., 2003. Methane bubbles in Lake Kinneret: Quantification and temporal and spatial heterogeneity. Limnol. Oceanogr. 48, 1030–1036. https://doi.org/10.4319/lo.2003.48.3.1030

Ostrovsky, I., McGinnis, D.F., Lapidus, L., Eckert, W., 2008. Quantifying gas ebullition with echosounder: the role of methane transport by bubbles in a medium-sized lake. Limnol. Oceanogr. Methods 6, 105–118. https://doi.org/10.4319/lom.2008.6.105

R Core Team, 2019. R Development Core Team. R: A language and environment for statistical computing (R Foundation for Statistical Computing, 2021).

Reeburgh, W.S., 1969. Observations of Gases in Chesapeake Bay Sediments1. Limnol. Oceanogr. 14, 368–375. https://doi.org/10.4319/lo.1969.14.3.0368

Rosentreter, J.A., Borges, A.V., Deemer, B.R., Holgerson, M.A., Liu, S., Song, C., Melack, J., Raymond, P.A., Duarte, C.M., Allen, G.H., Olefeldt, D., Poulter, B., Battin, T.I., Eyre, B.D., 2021. Half of global methane emissions come from highly variable aquatic ecosystem sources. Nat. Geosci. 14, 225–230. https://doi.org/10.1038/s41561-021-00715-2

Sander, R., 2015. Compilation of Henry's law constants (version 4.0) for water as solvent. Atmospheric Chem. Phys. 15, 4399–4981. https://doi.org/10.5194/acp-15-4399-2015

Scandella, B.P., Varadharajan, C., Hemond, H.F., Ruppel, C., Juanes, R., 2011. A conduit dilation model of methane venting from lake sediments: METHANE VENTING FROM LAKE SEDIMENTS. Geophys. Res. Lett. 38, n/a-n/a. https://doi.org/10.1029/2011GL046768

Sirhan, S.T., Katsman, R., Lazar, M., 2019. Methane Bubble Ascent within Fine-Grained Cohesive Aquatic Sediments: Dynamics and Controlling Factors | Environmental Science & Technology. Environ. Sci. Technol.

Vagle, S., McNeil, C., Steiner, N., 2010. Upper ocean bubble measurements from the NE Pacific and estimates of their role in air-sea gas transfer of the weakly soluble gases nitrogen and oxygen. J. Geophys. Res. Oceans 115. https://doi.org/10.1029/2009JC005990

Waldemer, C., Koschorreck, M., 2023. Spatial and temporal variability of greenhouse gas ebullition from temperate freshwater fish ponds. Aquaculture.

Weiland, P., 2010. Biogas production: current state and perspectives. Appl. Microbiol. Biotechnol. 85, 849–860. https://doi.org/10.1007/s00253-009-2246-7

Zhang, Y., Tang, K.W., Yang, P., Yang, H., Tong, C., Song, C., Tan, L., Zhao, G., Zhou, X., Sun, D., 2022. Assessing carbon greenhouse gas emissions from aquaculture in China based on aquaculture system types, species, environmental conditions and management practices. Agric. Ecosyst. Environ. 338, 108110. https://doi.org/10.1016/j.agee.2022.108110

Figure 1. Study site: (a) location close to Bautzen, Germany, (b) location of bubble traps (black dots) at the stationary feeding sites and 55 m towards the centre of ten fish ponds (investigated in Jun 2021) as well as the outline of the Gerstenteich fish pond (black solid line, investigated in Sep 2021). (c) Gerstenteich with symbols marking the locations of bubble traps (black dots, S01, S02 and S03) and optical bubble-sizers (open dots, B01 to B04). The feeding site with elevated ebullition rates is marked in grey (adapted from Waldemer and Koschorreck, 2023).

Figure 2. Methods used to measure bubble sizes in the Gerstenteich fish pond: (a) schematic of a bubble trap consisting of an inverted funnel (area: 0.14 m^2) and a syringe closed by a three-way valve and (b) schematic of a bubble-sizer designed according to Delwiche and Hemond (2017a) with attached inverted funnel (area: 0.06 m^2) which detected rising bubbles by three photoelectric sensors at a depth of about 35 cm.

Figure 3. Gerstenteich study results vs. time of the day in hours: (a) model-derived bubble diameter using dissolved gas concentrations at the beginning (dashed line) and at the end (solid line) of the sampling periods at S01 (bubble trap at feeding site), S02 and S03 (open water area). (b) Sauter mean diameters (SMD) of the measurements at bubble-sizers B01, B02, B03 and B04. (c) Ebullition rates at all sites. (d) Measured oxygen content in the collected bubble gas (errors due to measurement accuracy ~1% of measured value, not shown to avoid overloading Fig. 3d).

Figure 4. Model-derived bubble diameter vs. ebullition rate using data from the Gerstenteich (black, results via the dissolved O_2 concentrations at the beginning (triangles) and at the end (circles) of the 3 h sampling periods) and from the ten neighboring fish ponds (red). Regression curve and 95% confidence interval in red.

Supporting Information for

Bubble size estimated from bubble gas composition in a temperate freshwater fish pond

Carolin Waldemer[a,c], Michael Schwarz[b], Andreas Lorke[b], Bertram Boehrer[a], Matthias Koschorreck[a]

[a] Department of Lake Research, Helmholtz Centre for Environmental Research-UFZ, Brueckstrasse 3a, 39114 Magdeburg, Germany

[b] Institute for Environmental Sciences, University of Kaiserslautern-Landau, Germany

[c] Corresponding author: Helmholtz Centre for Environmental Research-UFZ. E-mail address: carolin.waldemer@ufz.de

Content

Figures S.1 to S.8

Tables S.1 and S.7

Introduction

This supplement provides information via figures and tables supporting the methods and results chapter of the main text.

Supplementary Figure S.1. Photos from the Gerstenteich near Bautzen, Germany, in Sep 2021: (a) view of the feeding site from the shore (visible are the automatic pellet feeder and site S01 at the pol a *of the bubble traps, the feeding site and the shore from the sampling boat and (c) view of the open water area of the pond from the sampling boat.*

07.09.2021 S01

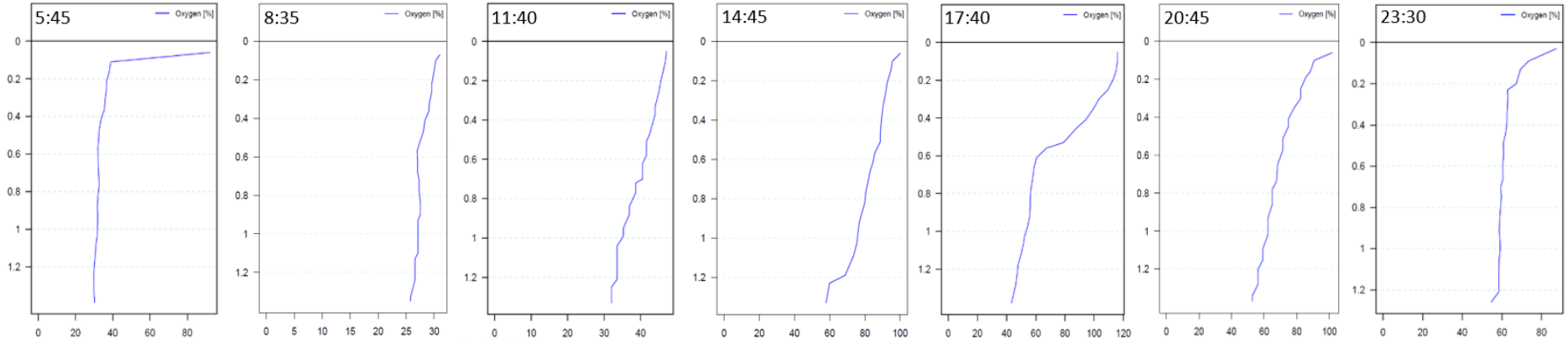

07.09.2021 S02

07.09.21 S05

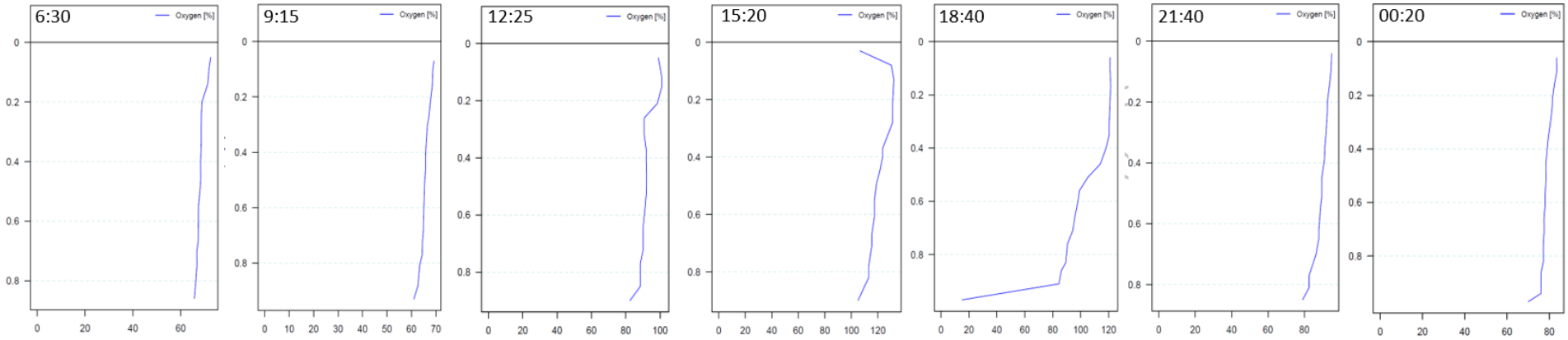

07.09.2021 S03

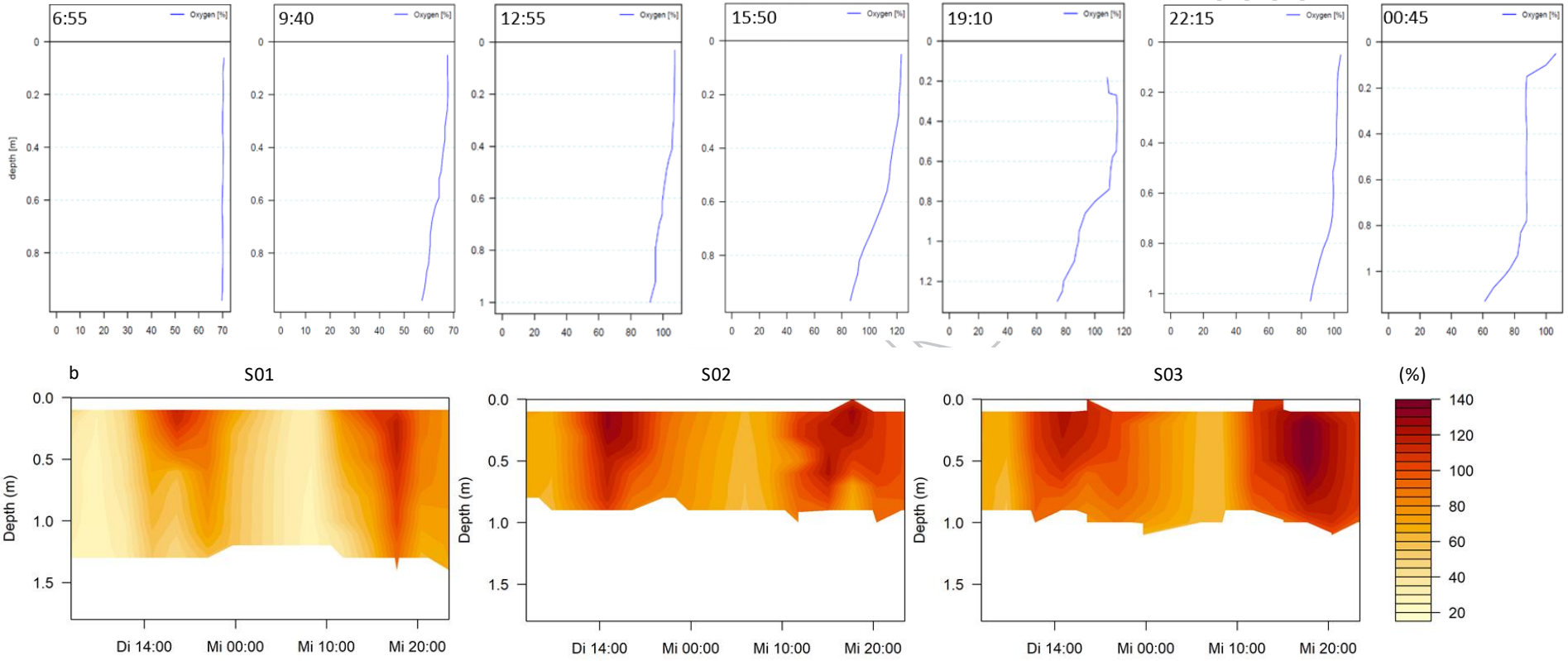

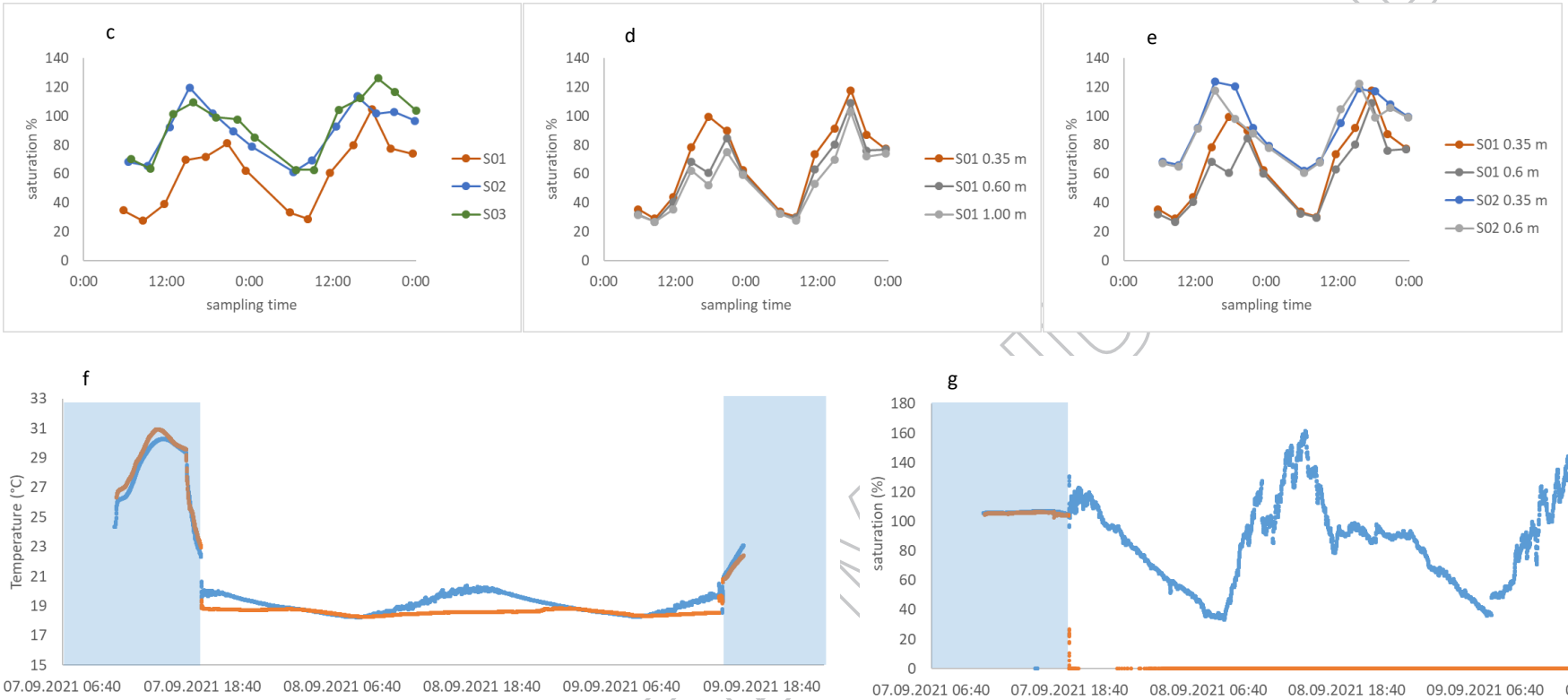

Supplementary Figure S.2. Gerstenteich, Sep 2021: (a) multiparameter probe profiles and (b) contour plots of dissolved oxygen saturation (100% means equilibration with the atmosphere oxygen content). Shown are the profiles of the sampling (PN) at 5:30, 11:30, 17:30 and 23:30 on 07.09.21 (PN01, PN03, PN05, PN07) and 08.09.21 (PN08, PN10, PN12, PN14) at the sites S01 and S03 as well as contour plots at the sites S01, S02 and S03 over the two sampling days. (c) Mean dissolved oxygen saturation of profiles and (d & e) saturation in specific depths for the different sites over the two days. (f) Logged dissolved oxygen and (g) water temperature in 35 cm depth (blue) and close to the sediment (red) at a site close to S02. Period before and after the sampling period shaded.

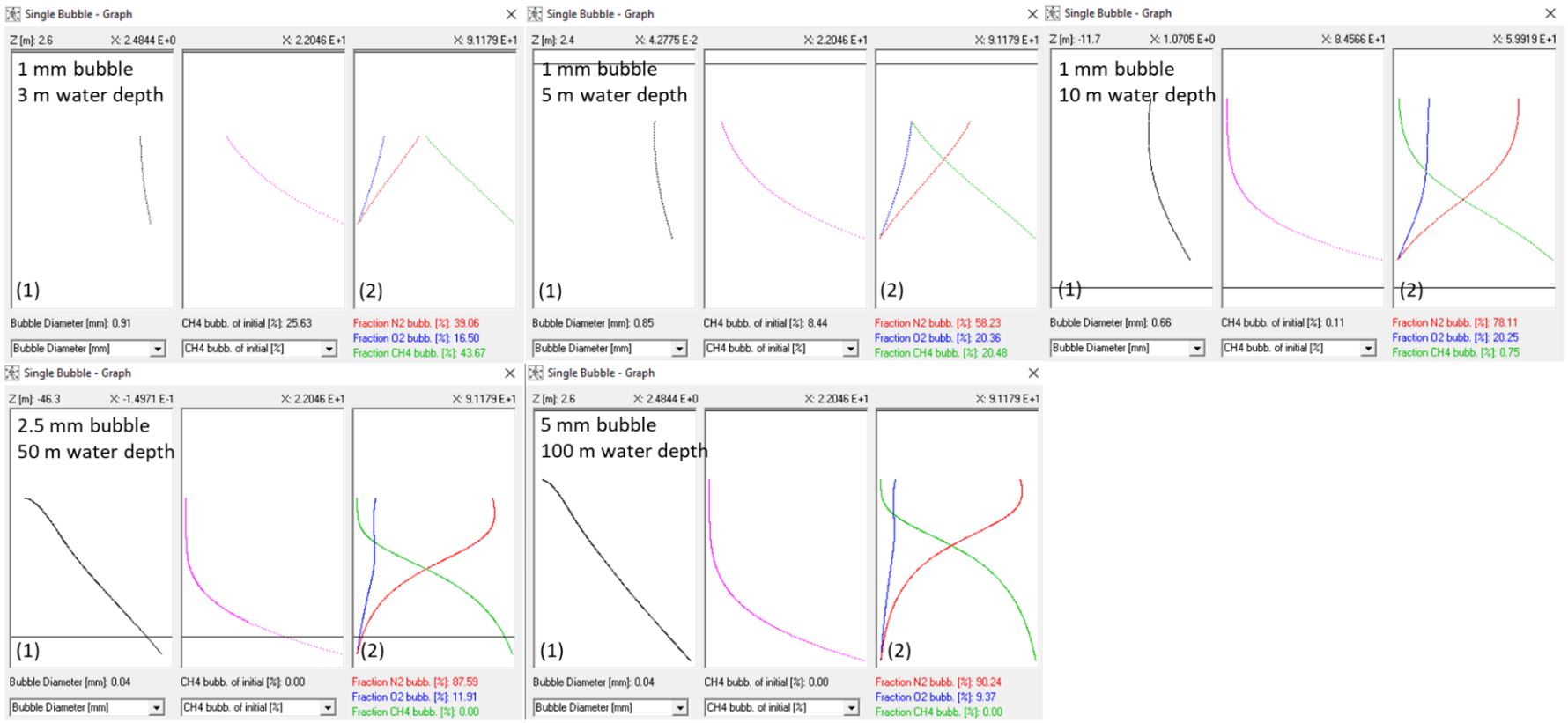

Supplementary Figure S.3. Model results with changing (1) bubble diameter and (2) bubble gas composition during the ascent of a 1 mm, 2.5 mm and 5 mm big methane (CH_4) bubble released at a water depth of 3 m, 5 m, 10 m, 50 m or 100 m (Greinert and McGinnis, 2009). Gerstenteich mean values of temperature, salinity, dissolved CH_4 and carbon dioxide concentrations and a dissolved oxygen (O_2) saturation of 100% were used as a basis for the model. The model assumes dissolved nitrogen (N_2) to be in equilibrium with the atmosphere. The development of the bubble O_2 content is shown in blue, bubble N_2 and CH_4 contents are given in red and green. The bubble gas contents at the water surface are given in %; the bubble diameter at the water surface is given in mm. 0.04 mm is the smallest bubble diameter possible in the model and indicates bubble dissolution.

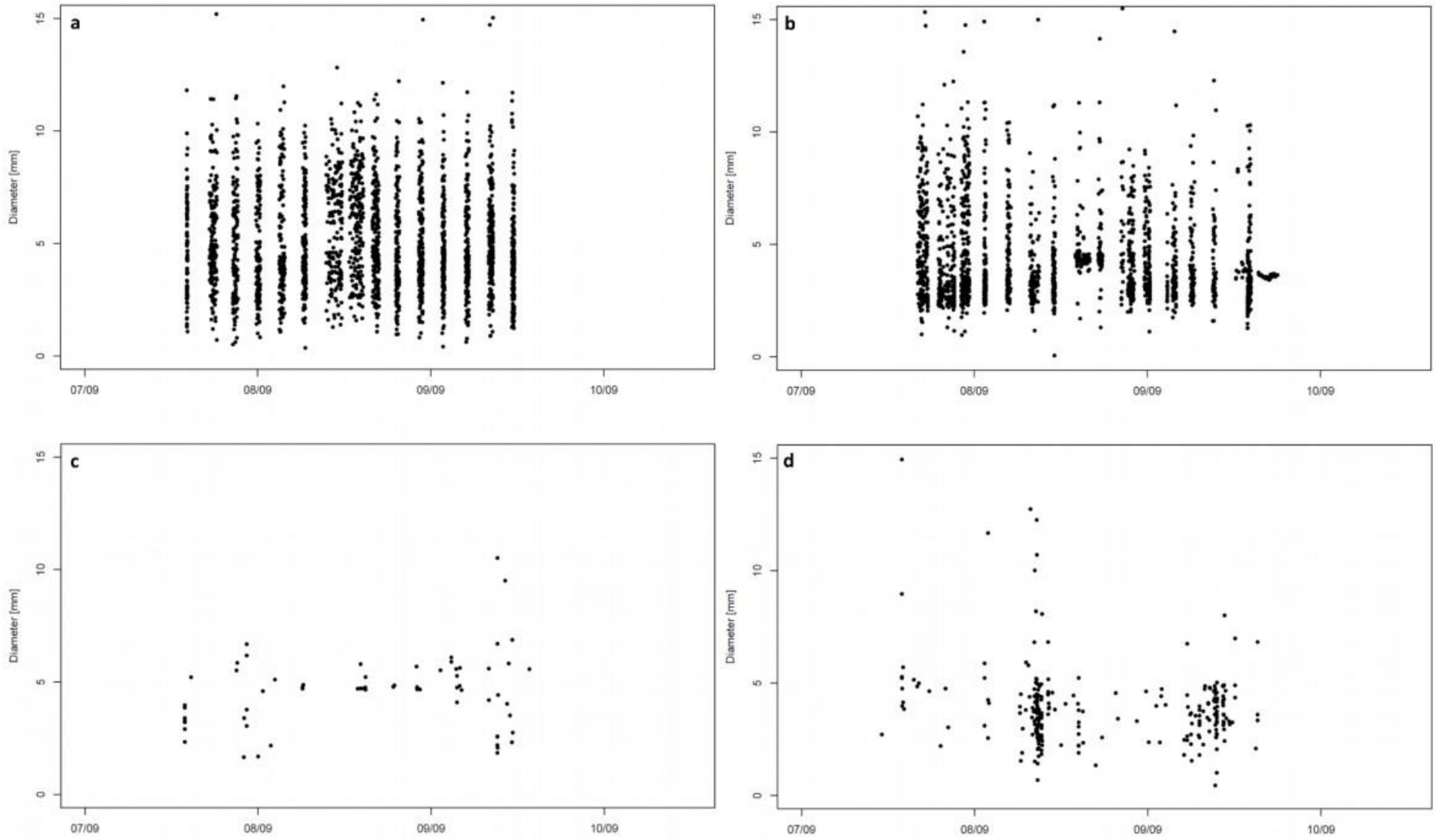

Supplementary Figure S.4. Correctly detected bubble events by the bubble-sizers for B01 (a) and B02 (b) at the feeding site and B03 (c) and B04 (d) in the center of the pond. Particularly visible at B01 and B02 are sections in which no further bubbles could be detected.

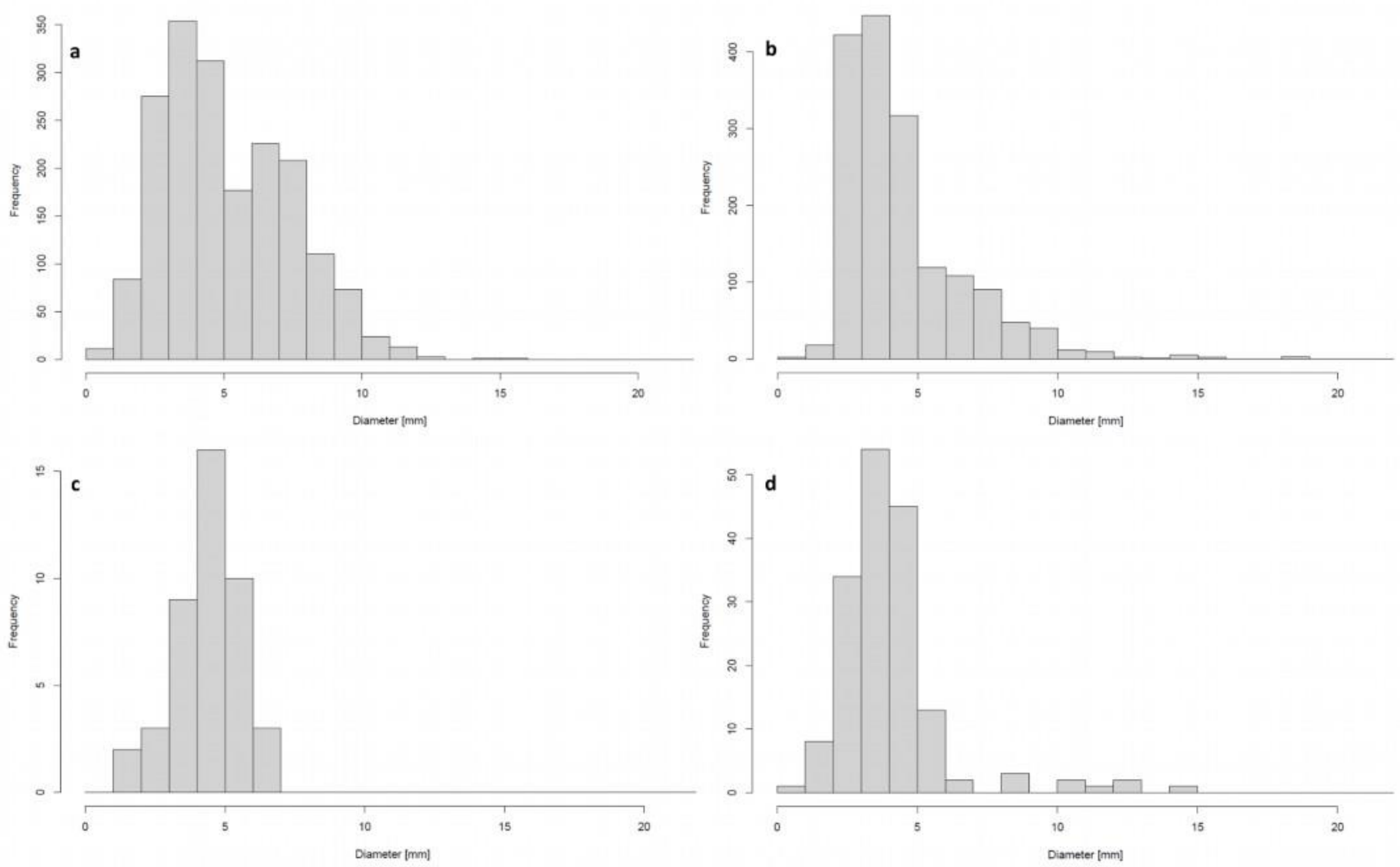

Supplementary Figure S.5. Histograms of correctly detected bubbles at B01 (a) and B02 (b) at the feeding site and B03 (c) and B04 (d) in the center of the pond on 07.09. and 08.09.2021.

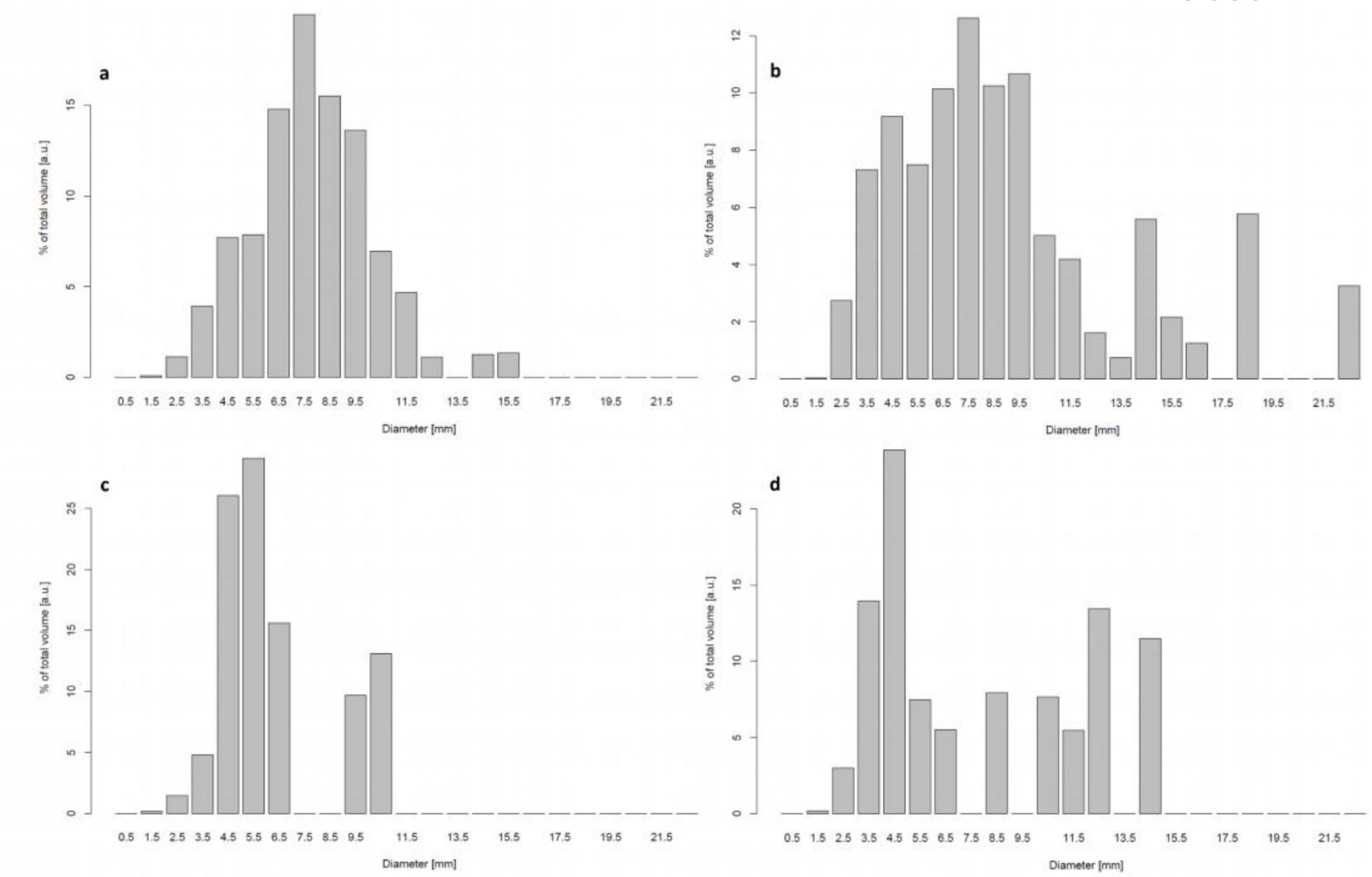

Supplementary Figure S.6. Volume fractions of correctly detected bubbles at B01 (a) and B02 (b) at the feeding site and B03 (c) and B04 (d) in the center of the pond on 07.09. and 08.09.2021.

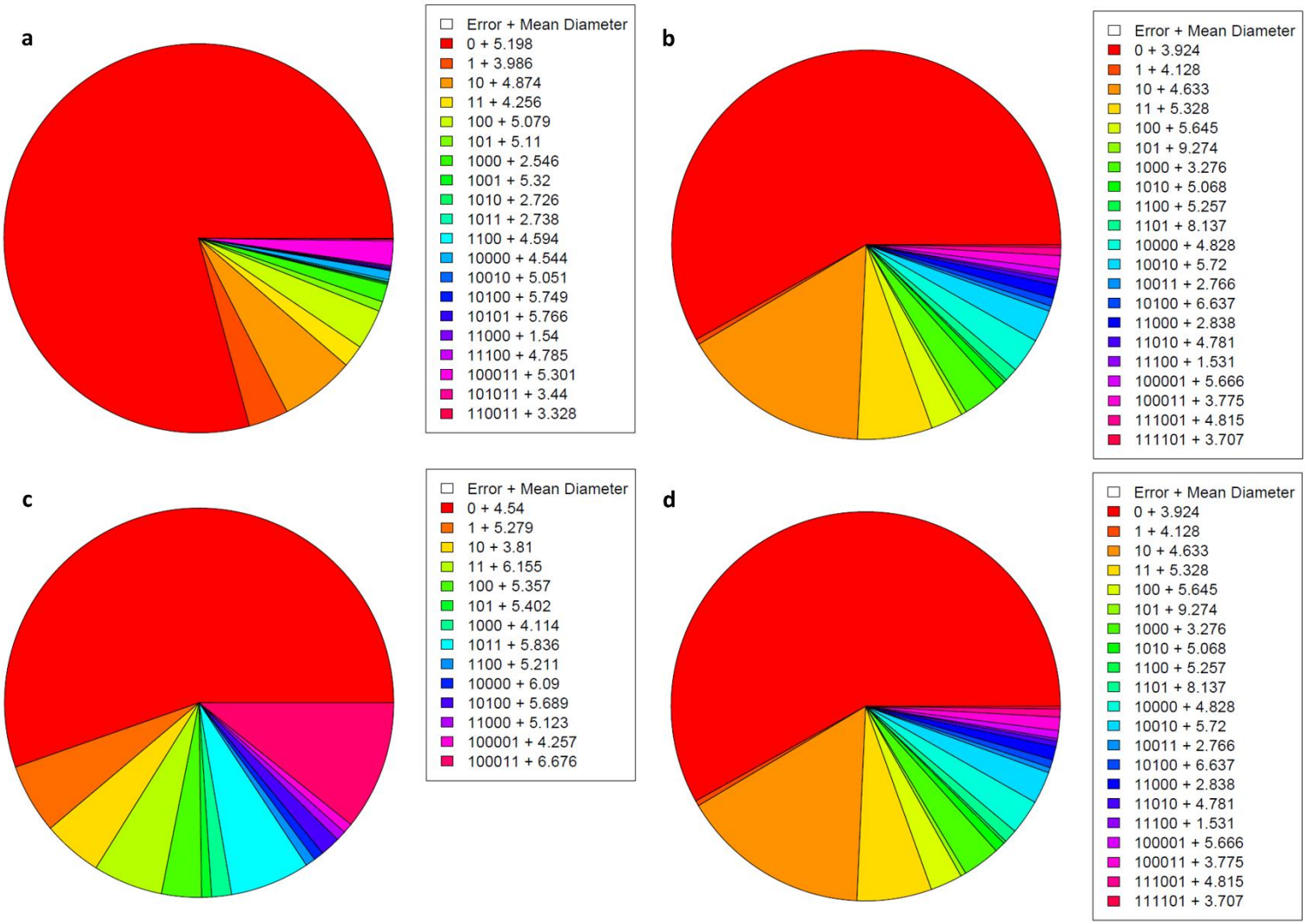
a
Error + Mean Diameter
0 + 5.198
1 + 3.986
10 + 4.874
11 + 4.256
100 + 5.079
101 + 5.11
1000 + 2.546
1001 + 5.32
1010 + 2.726
1011 + 2.738
1100 + 4.594
10000 + 4.544
10010 + 5.051
10100 + 5.749
10101 + 5.766
11000 + 1.54
11100 + 4.785
100011 + 5.301
101011 + 3.44
110011 + 3.328
b
Error + Mean Diameter
0 + 3.924
1 + 4.128
10 + 4.633
11 + 5.328
100 + 5.645
101 + 9.274
1000 + 3.276
1010 + 5.068
1100 + 5.257
1101 + 8.137
10000 + 4.828
10010 + 5.72
10011 + 2.766
10100 + 6.637
11000 + 2.838
11010 + 4.781
11100 + 1.531
100001 + 5.666
100011 + 3.775
111001 + 4.815
111101 + 3.707
c
Error + Mean Diameter
0 + 4.54
1 + 5.279
10 + 3.81
11 + 6.155
100 + 5.357
101 + 5.402
1000 + 4.114
1011 + 5.836
1100 + 5.211
10000 + 6.09
10100 + 5.689
11000 + 5.123
100001 + 4.257
100011 + 6.676
d
Error + Mean Diameter
0 + 3.924
1 + 4.128
10 + 4.633
11 + 5.328
100 + 5.645
101 + 9.274
1000 + 3.276
1010 + 5.068
1100 + 5.257
1101 + 8.137
10000 + 4.828
10010 + 5.72
10011 + 2.766
10100 + 6.637
11000 + 2.838
11010 + 4.781
11100 + 1.531
100001 + 5.666
100011 + 3.775
111001 + 4.815
111101 + 3.707

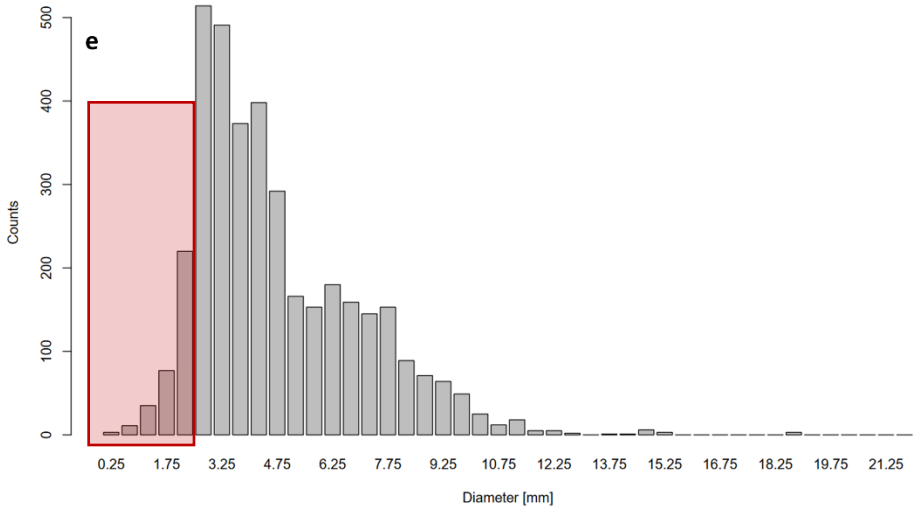
e
Counts
0
100
200
300
400
500
0.25
1.75
3.25
4.75
6.25
7.75
9.25
10.75
12.25
13.75
15.25
16.75
18.25
19.75
21.25
Diameter [mm]

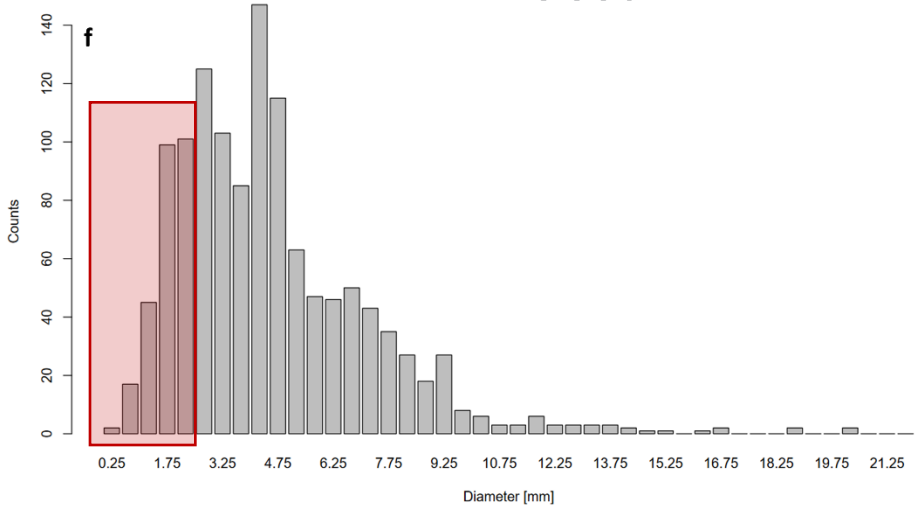
f
Counts
0
20
40
60
80
100
120
140
0.25
1.75
3.25
4.75
6.25
7.75
9.25
10.75
12.25
13.75
15.25
16.75
18.25
19.75
21.25
Diameter [mm]

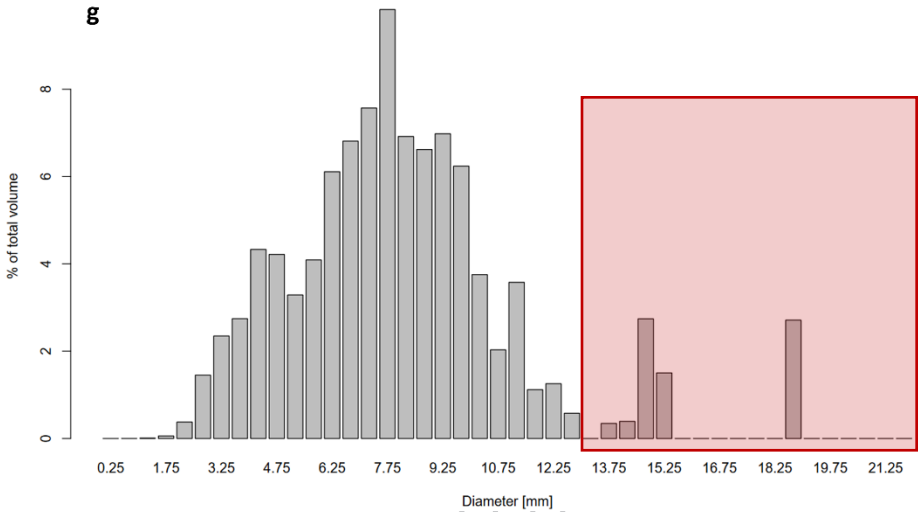
g
% of total volume
0
2
4
6
8
0.25
1.75
3.25
4.75
6.25
7.75
9.25
10.75
12.25
13.75
15.25
16.75
18.25
19.75
21.25
Diameter [mm]

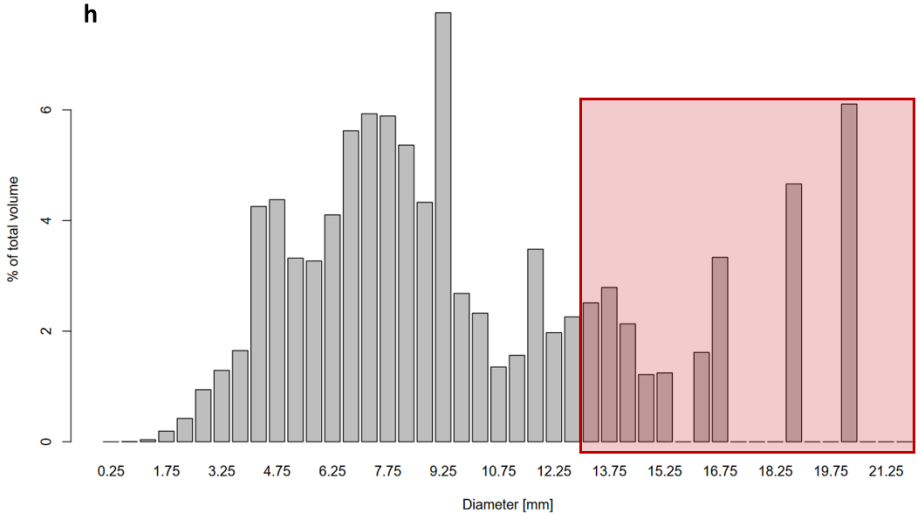
h
% of total volume
0
2
4
6
0.25
1.75
3.25
4.75
6.25
7.75
9.25
10.75
12.25
13.75
15.25
16.75
18.25
19.75
21.25
Diameter [mm]

Supplementary Figure S.7. Evaluation of bubble-sizer field data: (a-d) results with error code + mean bubble diameter (mm): correctly detected bubbles in red (error code 0), bubbles detected according to one of seven error codes or their combination in different colours (s. Delwiche and Hemond, 2017) for B01 (a) and B02 (b) at the feeding site and B03 (c) and B04 (d) in the center of the pond. (e-f) Histograms of all data collected in the field: (e) histogram of correct detections and (f) histogram to erroneous detections (the deviations in the distribution pattern in the area of the bubbles < 2 mm are marked). (g) Histogram to the volume contribution of correct detections and (h) histogram to the volume contribution of erroneous detections (the deviations in the distribution pattern in the area of the bubbles ≥ 13 mm are marked).

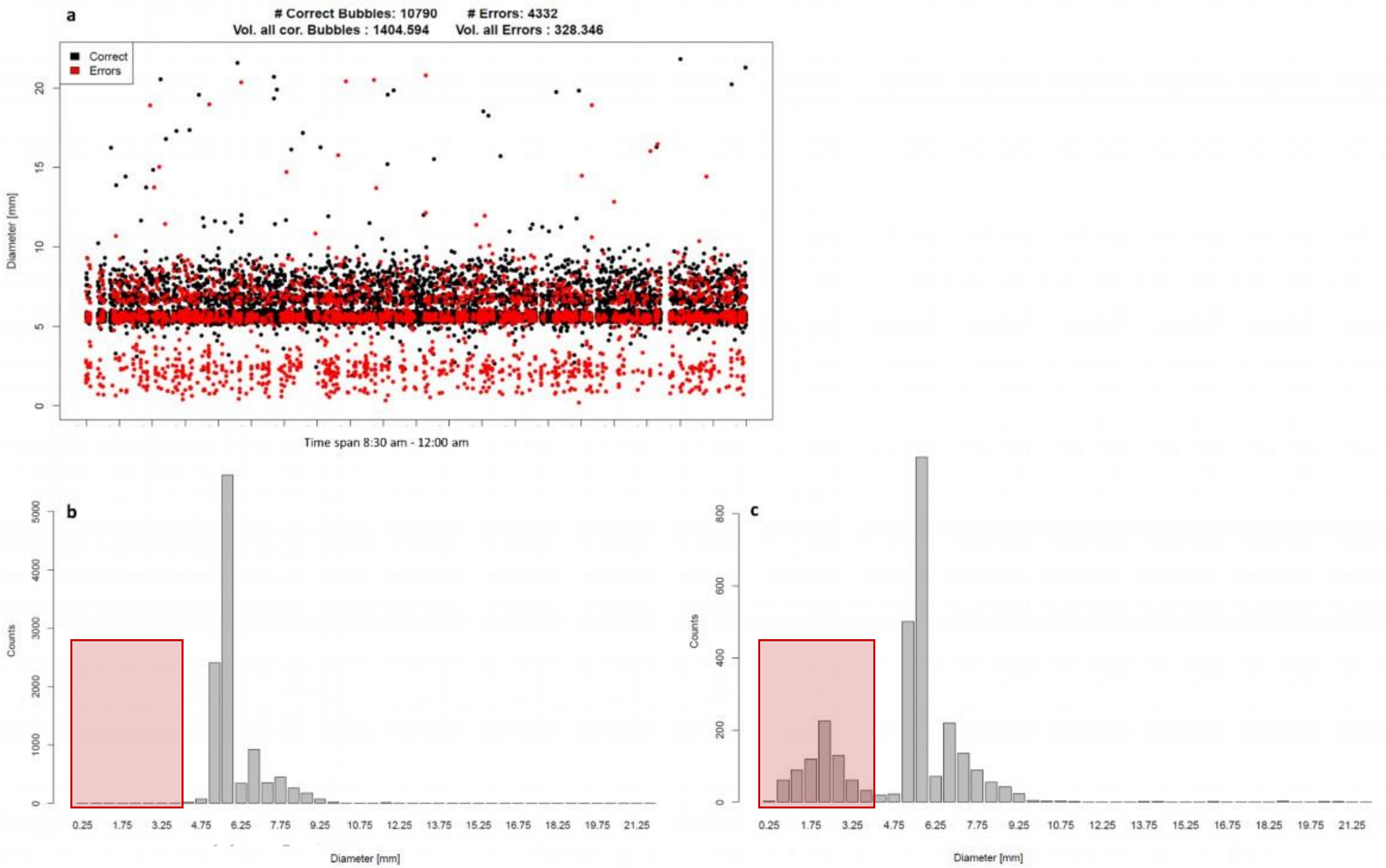
a
Correct Bubbles: 10790
Errors: 4332
Vol. all cor. Bubbles : 1404.594
Vol. all Errors : 328.346
Correct
Errors
Diameter [mm]
Time span 8:30 am - 12:00 am
b
Counts
Diameter [mm]
c
Counts
Diameter [mm]

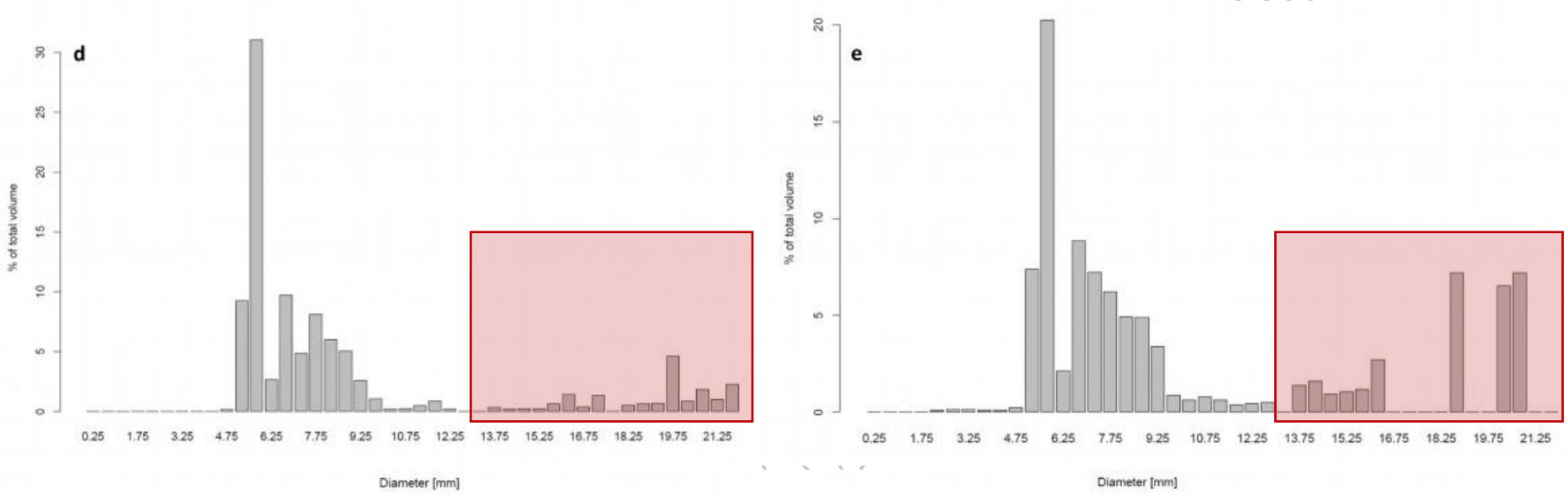

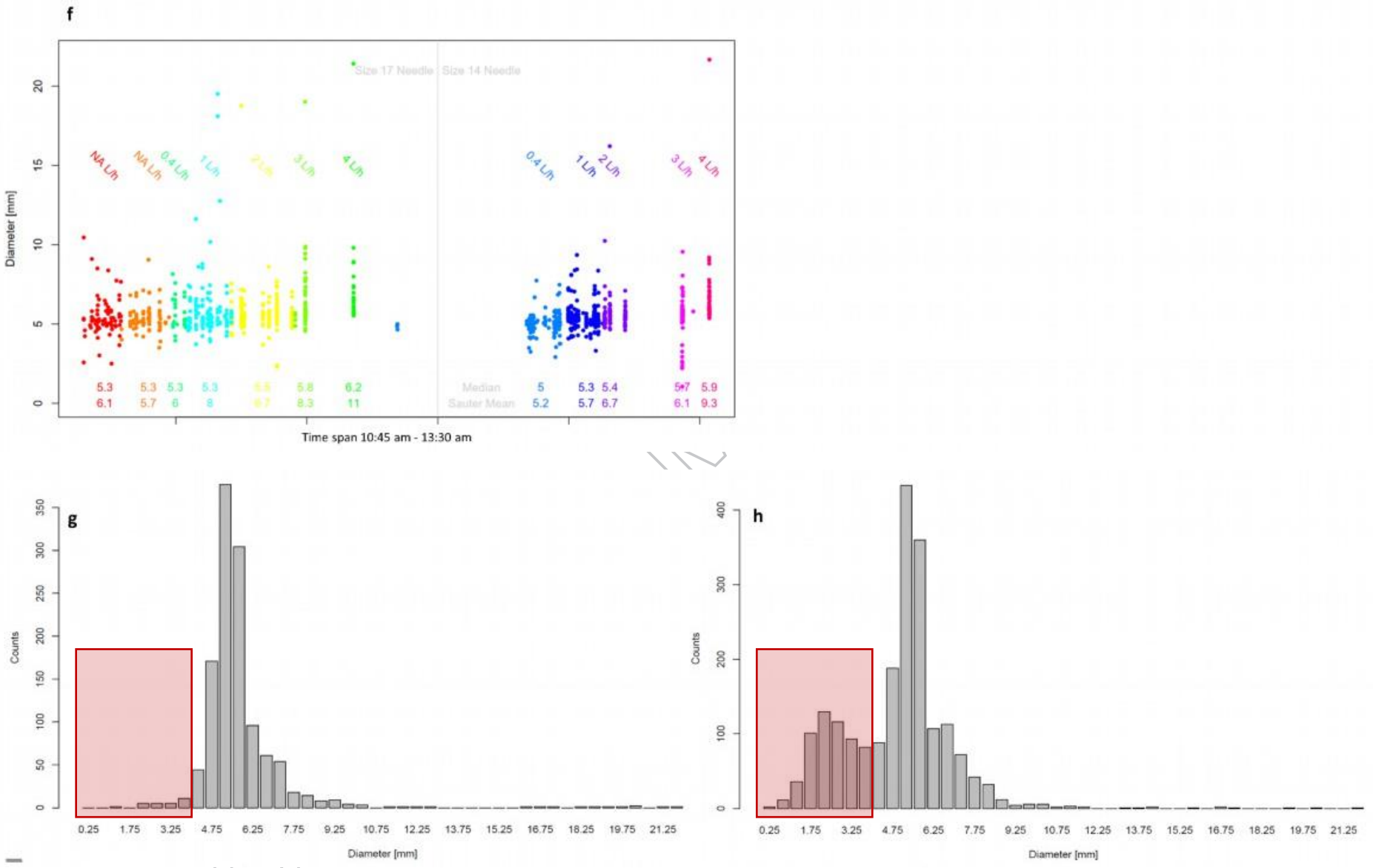
f
Size 17 Needle | Size 14 Needle
Diameter [mm]
NA L/h
NA L/h
0.4 L/h
1 L/h
2 L/h
3 L/h
4 L/h
0.4 L/h
1 L/h
2 L/h
3 L/h
4 L/h
Median
Sauter Mean
Time span 10:45 am - 13:30 am
g
Counts
Diameter [mm]
h
Counts
Diameter [mm]

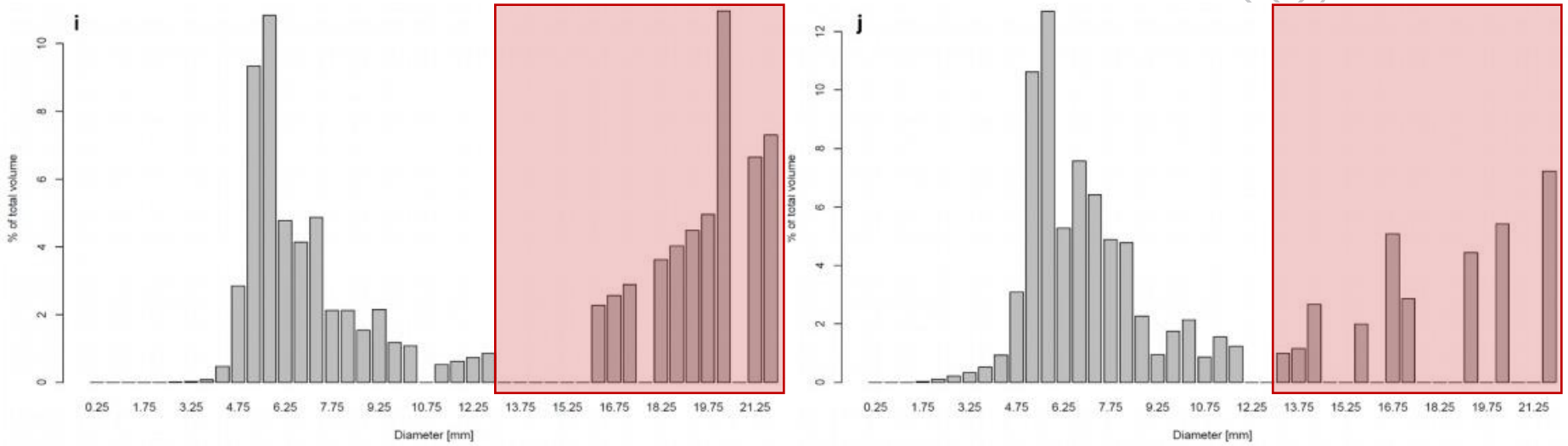

Supplementary Figure S.8. Evaluation of bubble-sizer laboratory experiments: (a-e) experiment with a constant pump rate of 1 L/h. (a) Detected bubble size over for 3.5h. Given is the total numbers of correctly detected bubble events (black) and erroneous detections (red) as well as their gas volume (mL) under the assumption of spherical bubbles. (b) Histogram of correct detections and (c) histogram to erroneous detections (the deviations in the distribution pattern in the area of the bubbles < 4 mm are marked). (d) Histogram to the volume contribution of correct detections and (e) histogram to the volume contribution of erroneous detections (the deviations in the distribution pattern in the area of the bubbles ≥ 13 mm are marked). (f-j) Experiments with two syringe needles of 0.60 mm and 0.55 mm inner diameter. Bubbles were created with a peristaltic pump at rates of 0.4, 1.0, 2.0, 3.0, 4.0 L/h. (f) Bubbles of one colour corresponds to one bubble rate as well as one needle size. The arithmetic means and Sauter mean diameters are displayed at the bottom in the colour corresponding to the bubbles. (g) Histogram of correct detections and (h) histogram to erroneous detections (the deviations in the distribution pattern in the area of the bubbles < 4 mm are marked). (i) Histogram to the volume contribution of correct detections and (j) histogram to the volume contribution of erroneous detections (the deviations in the distribution pattern in the area of the bubbles ≥ 13 mm are marked).

Supplementary Table S.1. Gerstenteich, Sep 2021: given are the ebullition rate, measured bubble gas composition (including methane (CH_4), carbon dioxide (CO_2), nitrogen (N_2), oxygen (O_2) and argon (Ar) concentrations), model-derived results of bubble diameter and bubble gas composition (initial and at the water surface) using the site-specific data at the beginning and the end of the sampling periods as well as the mean bubble diameter at the water surface in mm. Site specific mean values ± standard deviations. For comparison, the averaged results of the evaluation assuming an initially pure CH_4 bubble are also given.

								Model results based on data at the beginning of the sampling period									Model results based on data at the end of the sampling period									Surface diameter	
Sampling	Ebullition	Bubble gas composition						initial	composition initial			surface	composition surface				initial	composition initial			surface	composition surface				gas comp.	100% CH_4
time	ml/m²d	CH_4%	CO_2%	N_2%	O_2%	Ar%	sum%	mm	CH_4%	CO_2%	N_2%	mm	CH_4%	CO_2%	N_2%	O_2%	mm	CH_4%	CO_2%	N_2%	mm	CH_4%	CO_2%	N_2%	O_2%	mm	mm
S01																											
7.9.21 5:45	30638	83	5	8	1.43	0.2	97										5.27	63	34	4	4.86	85	5	8	1.43	4.9	4.7
7.9.21 8:35	38212	80	14	7	0.49	0.2	102	5.75	48	50	3	4.95	81	11	8	0.49	6.10	52	47	3	5.42	80	12	8	0.49	5.2 ± 0.3	5 ± 0.1
7.9.21 11:40	27361	75	16	7	0.64	0.2	100	5.90	36	63	2	4.68	76	16	7	0.64	7.09	48	49	3	6.27	76	16	7	0.64	5.5 ± 1.1	4.8 ± 1.1
7.9.21 14:45	32249	82	10	7	0.78	0.2	101	5.75	53	45	2	5.08	82	10	7	0.78	9.28	70	26	4	9.11	82	11	6	0.78	7.1 ± 2.8	6.9 ± 2.6
7.9.21 17:40	50722	81	11	8	0.82	0.2	101	8.70	70	24	6	8.56	81	9	9	0.82	10.30	73	21	6	10.3	81	9	8	0.82	9.4 ± 1.2	9.2 ± 1.2
7.9.21 20:45	56520	78	17	7	0.92	0.1	103	9.70	64	31	5	9.43	78	14	7	0.92	8.90	61	35	4	8.49	78	14	7	0.92	9 ± 0.7	8.5 ± 0.8
7.9.21 23:25	49695	74	16	7	0.94	0.2	98	8.70	57	38	5	8.21	75	16	8	0.94	9.25	56	41	4	8.71	74	18	7	0.94	8.5 ± 0.4	8 ± 0.2
8.9.21 5:45	40508	76	11	6	1.68	0.4	95	6.00	50	48	3	5.28	79	12	7	1.68	5.51	43	55	2	4.57	80	10	8	1.68	4.9 ± 0.5	4.5 ± 0.8
8.9.21 8:25	43004	76	18	6	0.66	0.2	100	8.40	55	42	3	7.77	77	17	6	0.83	5.66	28	72	0	4.12	76	17	6	0.83	5.9 ± 2.6	5.1 ± 2.9
8.9.21 11:35	35831	74	16	5	0.74	0.1	96	5.65	32	67	1	4.3	77	16	7	0.74	8.10	60	36	5	8.45	76	16	7	0.74	6.4 ± 2.9	6 ± 3.5
8.9.21 14:55	40588	80	14	6	0.72	0.1	101	9.20	66	31	4	8.92	80	13	6	0.72	10.60	70	26	4	10.49	81	13	6	0.72	9.7 ± 1.1	9.5 ± 1.1
8.9.21 17:37	30155	80	12	8	0.97	0.2	101	8.59	65	30	5	8.31	79	12	8	0.97	8.60	67	28	5	8.38	80	11	8	0.97	8.3 ± 0	8.1 ± 0.1
8.9.21 20:20	39407	82	11	6	0.81	0.1	101	9.80	71	25	4	9.7	82	11	6	0.81	8.60	69	27	4	8.38	82	10	7	0.81	9 ± 0.9	8.8 ± 1
8.9.21 23:30	44693	83	10	6	0.96	0.2	100	7.60	67	30	3	7.28	83	10	6	0.96	6.95	64	33	3	6.55	83	10	6	0.96	6.9 ± 0.5	6.6 ± 0.6
9.9.21 0:30	20788	74	13	9	0.96	0.4	97	7.25	55	40	5	6.68	77	13	9	0.96	7.20	55	39	6	6.66	76	12	11	0.96	6.7 ± 0	6.2 ± 0
	38691 ± 9570	**79 ± 4**	**13 ± 3**	**7 ± 1**	**0.9 ± 0.3**	**0.2 ± 0.1**	**99 ± 2**	**7.6 ± 1.6**	**56 ± 12**	**40 ± 13**	**3 ± 1**	**7.1 ± 1.9**	**79 ± 3**	**13 ± 3**	**7 ± 1**	**0.9 ± 0.3**	**7.8 ± 1.7**	**59 ± 12**	**38 ± 13**	**4 ± 2**	**7.4 ± 2**	**79 ± 3**	**12 ± 3**	**7 ± 1**	**0.9 ± 0.3**	**7.2 ± 1.9**	**6.9 ± 2**
S02																											
7.9.21 6:30	244	45	0.5	48	3.88	0.7	98										1.35	57	0	43	1.36	45	0.7	50	3.9	1.4	1.4
7.9.21 9:15	441	47	0.0	50	2.35	0.8	100	1.98	54	0	46	2.02	47	0.6	50	2.35	1.90	54	0	46	1.95	47	0.6	50	2.4	2 ± 0	2 ± 0
7.9.21 12:25	602	56	0.1	39	3.09	0.7	99	1.56	68	0	32	1.58	57	0.7	39	3.09	2.05	65	0	35	2.1	57	0.3	40	3.1	1.8 ± 0.4	1.9 ± 0.4
7.9.21 18:40	97	45	0.0	47	6.81	0.7	99	1.11	62	0	38	1.12	45	0.5	48	6.81	1.28	60	0	40	1.3	45	0.3	47	6.8	1.2 ± 0.1	1.2 ± 0.1
8.9.21 6:20	144	46	0.0	50	1.63	0.8	98	3.10	51	0	49	3.19	47	0.4	51	1.63	2.39	52	0	48	2.46	47	0.7	51	1.6	2.8 ± 0.5	2.9 ± 0.5
8.9.21 12:30	198	44	0.0	44	7.35	0.9	96	0.89	69	0	31	0.88	46	0.9	46	7.35	1.02	66	0	34	1.02	46	0.6	46	7.4	1 ± 0.1	1 ± 0.1
8.9.21 15:33	142	47	0.0	42	6.46	0.9	97	1.12	66	0	34	1.13	49	0.6	44	6.46	1.23	65	0	35	1.24	49	0.4	44	6.5	1.2 ± 0.1	1.2 ± 0.1
8.9.21 23:51	73	50	0.1	43	5.93	0.5	100	1.32	65	0	35	1.33	51	0.4	43	5.93	1.26	66	0	34	1.27	51	0.6	43	5.9	1.3 ± 0	1.3 ± 0
	243 ± 185	**47 ± 4**	**0.1 ± 0.2**	**45 ± 4**	**4.7 ± 2.2**	**0.8 ± 0.2**	**98 ± 1**	**1.6 ± 0.8**	**62 ± 7**	**0**	**38 ± 7**	**1.6 ± 0.8**	**49 ± 4**	**0.6 ± 0.2**	**46 ± 4**	**4.8 ± 2.4**	**1.6 ± 0.5**	**61 ± 6**	**0**	**39 ± 6**	**1.6 ± 0.5**	**48 ± 4**	**0.5 ± 0.2**	**46 ± 4**	**4.7 ± 2.2**	**1.6 ± 0.6**	**1.6 ± 0.6**

S03																										
7.9.21 6:55	62	30	0.0	62	6.84	0.8	99										0.83	50	0	50	0.82	31	0.9	62	6.8	0.8	0.9
7.9.21 9:40	220	36	0.0	55	5.27	0.9	97	1.03	53	0	47	1.03	37	0.8	57	5.27	0.99	53	0	47	1	37	0.8	57	5.3	1 ± 0	1 ± 0
7.9.21 12:55	107	33	0.0	56	8.66	0.9	99	0.66	65	0	35	0.64	34	1.0	57	8.66	0.94	52	0	48	0.95	33	0.6	57	8.7	0.8 ± 0.2	0.8 ± 0.2
7.9.21 22:15	121	48	0.0	47	5.36	0.9	101	1.55	59	0	41	1.58	48	0.2	47	5.36	1.39	60	0	40	1.41	47	0.5	47	5.4	1.5 ± 0.1	1.5 ± 0.1
8.9.21 6:40	84	50	0.1	48	3.02	0.9	102	2.16	57	0	43	2.22	50	0.4	47	3.02	1.48	61	0	39	1.5	50	0.8	46	3.0	1.9 ± 0.5	1.8 ± 0.5
8.9.21 9:15	469	49	0.0	46	4.11	0.8	100	1.17	64	0	36	1.17	49	0.9	46	4.11	1.17	64	0	36	1.17	49	0.8	46	4.1	1.2 ± 0	1.2 ± 0
8.9.21 12:50	169	42	0.0	43	9.88	1.1	96	0.60	90	0	10	0.54	44	1.2	45	9.87	0.86	69	0	31	0.86	43	0.7	46	9.9	0.7 ± 0.2	0.7 ± 0.2
8.9.21 15:58	138	34	0.0	52	11.90	0.9	98	0.73	63	0	37	0.72	34	0.8	54	11.90	0.72	65	0	35	0.71	34	0.6	53	11.9	0.7 ± 0	0.7 ± 0
9.9.21 0:00	52	40	0.0	51	7.22	0.8	99	1.09	57	0	43	1.1	40	0.4	52	7.22	1.12	57	0	43	1.13	41	0.6	52	7.2	1.1 ± 0	1.1 ± 0
	158 ± 128	**40 ± 7**	**0 ± 0**	**51 ± 6**	**6.9 ± 2.8**	**0.9 ± 0.1**	**99 ± 2**	**1.1 ± 0.5**	**64 ± 11**	**0**	**37 ± 11**	**1.1 ± 0.6**	**42 ± 7**	**0.7 ± 0.3**	**50 ± 5**	**6.9 ± 3**	**1.1 ± 0.3**	**59 ± 6**	**0**	**41 ± 6**	**1.1 ± 0.3**	**41 ± 7**	**0.7 ± 0.1**	**52 ± 6**	**6.9 ± 2.9**	**1.1 ± 0.4**	**1.1 ± 0.4**
S02 & S03	**198 ± 158**	**44 ± 7**	**0 ± 0**	**48 ± 6**	**5.9 ± 2.7**	**0.8 ± 0.1**																				**1.3 ± 0.6**	**1.3 ± 0.6**

Supplementary Table S.2. Gerstenteich, Sep 2021: multiparameter probe profile means ± standard deviation for dissolved oxygen (O_2) concentration and saturation as well as dissolved oxygen O_2 concentration and saturation near the ground.

S01			S02			S03		
Sampling time	Dissolved O_2		Sampling time	Dissolved O_2		Sampling time	Dissolved O_2	
	mg L^{-1}	%		mg L^{-1}	%		mg L^{-1}	%
07.09.2021 05:45	3.3 ± 1.1	35 ± 11.7	07.09.2021 06:30	6.4 ± 0.2	68.4 ± 1.9	07.09.2021 06:55	6.6 ± 0	70.1 ± 0.2
07.09.2021 08:35	2.6 ± 0.1	27.8 ± 1.4	07.09.2021 09:15	6.1 ± 0.2	65.6 ± 2.1	07.09.2021 09:40	6 ± 0.3	63.7 ± 3.6
07.09.2021 11:40	3.6 ± 0.5	39.2 ± 5.1	07.09.2021 12:25	8.5 ± 0.4	92.4 ± 4.9	07.09.2021 12:55	9.3 ± 0.4	101.4 ± 5.3
07.09.2021 14:45	6.4 ± 1.1	69.7 ± 12.6	07.09.2021 15:20	10.9 ± 0.7	119.8 ± 8.8	07.09.2021 15:50	9.9 ± 1	109.5 ± 12.9
07.09.2021 17:40	6.5 ± 2.3	71.9 ± 26.2	07.09.2021 18:40	9.3 ± 2.3	101.9 ± 25.2	07.09.2021 19:10	9.1 ± 1.3	99 ± 14.8
07.09.2021 20:45	7.6 ± 1.1	81.3 ± 11.4	07.09.2021 21:40	8.3 ± 0.4	89.2 ± 4.5	07.09.2021 22:15	9.1 ± 0.5	97.7 ± 5.6
07.09.2021 23:25	5.8 ± 0.7	62.2 ± 6.6	08.09.2021 00:20	7.3 ± 0.3	78.7 ± 3.1	08.09.2021 00:45	7.9 ± 0.9	85.2 ± 9.5
08.09.2021 05:45	3.1 ± 0.1	33.4 ± 1.1	08.09.2021 06:20	5.8 ± 0.2	61.3 ± 1.7	08.09.2021 06:40	5.9 ± 0	62.8 ± 0.4
08.09.2021 08:25	2.7 ± 0.1	28.9 ± 1.5	08.09.2021 09:00	6.5 ± 0.6	69.5 ± 6.1	08.09.2021 09:15	5.9 ± 0.1	62.9 ± 0.8
08.09.2021 11:35	5.6 ± 1.4	60.9 ± 15.4	08.09.2021 12:30	8.5 ± 1.1	92.9 ± 12.4	08.09.2021 12:50	9.3 ± 0.3	104.3 ± 4.5
08.09.2021 14:55	7.2 ± 1.2	79.9 ± 14.7	08.09.2021 15:33	10.2 ± 0.8	113.6 ± 9.4	08.09.2021 15:58	10.1 ± 1.1	112.3 ± 13.5
08.09.2021 17:37	9.4 ± 0.8	104.7 ± 10.1	08.09.2021 18:16	9.2 ± 2	101.8 ± 22.7	08.09.2021 18:30	11.4 ± 1.3	126.2 ± 15.9
08.09.2021 20:20	7.1 ± 0.8	77.7 ± 9.6	08.09.2021 20:48	9.5 ± 0.5	103 ± 6.2	08.09.2021 20:57	10.7 ± 1	116.5 ± 11.1
08.09.2021 23:30	6.9 ± 0.4	74 ± 4.7	08.09.2021 23:51	9 ± 0.5	96.7 ± 5.8	09.09.2021 00:00	9.6 ± 0.7	103.8 ± 7.6
Mean profile	5.6 ± 2.1	60.5 ± 23.8	Mean profile	8.3 ± 1.6	89.6 ± 18.4	Mean profile	8.6 ± 1.9	94 ± 21.4
At ground level	4.3 ± 1.5	46.5 ± 17.1	At ground level	6.5 ± 1.8	70.0 ± 21.2	At ground level	6.8 ± 1.0	74.7 ± 11.2

Supplementary Table S.3. Selection of chemical and physical water, pore water and sediment parameters of the Gerstenteich, Sep 2021 (further parameters and details regarding sampling and analysis in Waldemer and Koschorreck, 2023). Given are the water temperature, salinity, conductivity, turbidity, chlorophyll a (mean values of the water column / values near the ground ± standard

deviation). Pore water concentrations of dissolved organic carbon (DOC), total bound nitrogen (TN_b) and sulphate (SO_4). Microbial available ferric iron (Fe) in wet sediment. Sediment particular organic carbon (POC) and sediment porosity. For both, the upper 5 cm of the sediment was sampled. DW abbreviated for dry weigh, SW for sediment wet weight. Concentrations below the limit of quantitation expressed like < limit of quantitation.

Gerstenteich site	**Temperature** (°C)	**Temp. at ground** (°C)	**Salinity** (PSU)	**Conductivity** (mS cm^{-1})	**Turbidity** (FTU)	**Chlorophyll a** (µg L^{-1})
S01	19.0 ± 0.4	18.6 ± 0.4	0.180	0.30 ± 0.01	34.8 ± 6.8	60.9 ± 5.7
S02	19.0 ± 0.5	18.7 ± 0.5	0.178	0.30 ± 0.04	27.6 ± 6.0	65.5 ± 8.9
S03	19.2 ± 0.7	18.6 ± 0.7	0.178	0.30 ± 0.04	33.1 ± 39.9	49.1 ± 7.2
Gerstenteich site	**DOC** (mg L^{-1})	**TN_b** (mg L^{-1})	**$SO4^{2-}$** (mg L^{-1})	**Fe^{3+}** (mg kg^{-1} SW)	**POC** (g kg^{-1} DW)	**Porosity** (%)
S01	234.1	1834.1	5.28	172	56.2	58
S02	13.6	38.4	< 0.8	51	46.6	80
S03	7.9	30.3	< 0.8	132	42.6	78

Supplementary Table S.4. Sensitivity analysis regarding the oxygen (O_2) sensor accuracy of the used needle-type optode (Firesting, Pyroscience, Aachen, Germany) in the due to our O_2 measurements relevant range of 0.5% to 17% O_2. The accuracy depended on the O_2 concentration. Assuming an initial pure methane (CH_4) bubble and using the profile with the highest dissolved O_2 at the deepest site (S01), the initial bubble diameter and the bubble diameter at the water surface were determined via the model. The deviation of the model-derived bubble diameter at the water surface is given in mm and as a relative error.

			Model-derived bubble diameter			Deviation	
Settings		O_2% surface	initial	surface		surface diameter	
depth (m)	profile	(%)	(mm)	(mm)	O_2 (%)	(mm)	(%)
1.65	19.0, 0.18, PN12 S01	0.50	13.10	13.73	0.50		
		0.52	12.80	13.41	0.52	0.32	2.33
		0.48	13.40	14.05	0.48	0.32	2.33
1.65	19.0, 0.18, PN12 S01	1.00	7.60	7.94	1.00		
		1.02	7.50	7.83	1.02	0.11	1.39
		0.98	7.75	8.09	0.98	0.15	1.89
1.65	19.0, 0.18, PN12 S01	4.99	1.88	1.90	4.99		
		5.06	1.86	1.88	5.06	0.02	1.05
		4.94	1.90	1.92	4.94	0.02	1.05
1.65	19.0, 0.18, PN12 S01	10.00	1.10	1.07	10.00		
		10.11	1.09	1.06	10.11	0.01	0.93
		9.89	1.11	1.08	9.89	0.01	0.93
1.65	19.0, 0.18, PN12 S01	17.01	0.69	0.63	17.01		
		17.18	0.68	0.62	17.18	0.01	1.59
		16.83	0.70	0.63	16.83	0.00	0.00

*Supplementary Table S.5. Investigation of the model results by generating normally distributed bubble diameter spectra. The spectra were divided into bins of similar size and number. For the mean of each bin, the oxygen (O_2) content at the water surface was determined via the model, assuming initially pure methane (CH_4) bubbles. The O_2 content of the total gas volume was calculated and used to determine a model-derived representative bubble diameter for the bubble size spectrum. The deviation between model-derived diameter and Sauter mean diameter (SMD) according to De Swart et al. (1996) at the water surface is given in mm and as relative error in brackets (using the model to describe the size change during bubble rise). As a general basis for the model, Gerstenteich mean values of dissolved carbon dioxide and methane, water temperature and salinity, a water depth of 1.5 m and 100% dissolved O_2 saturation were used. In addition, the maximum and minimum dissolved O_2 profiles of site S02 (depth: 1.2 m) were used. We investigated the effect of different dissolved O_2 levels, bubble spectra, depth, temperature and salinity. *The relative standard deviation is 0.33%.*

		Normal distribution of initial bubble sizes				Model-derived bubble sizes at water surface			
Variable investigated	Dissolved O_2	Arithmetic mean, standard deviation	SMD	Number of bubbles	Classes (number, range, width)	O_2% of total gas volume	Bubble size via O_2%	Bubble size based on SMD	Deviation
Mean / Deviation	100% Sat	4.0 mm, 1.3 mm	4.8 mm	2000	9; 0.5 - 8.5; 1	1.54	5.0 mm	5.0 mm	0.1 mm (2%)
Mean / Deviation	100% Sat	6.0 mm, 1.3 mm	6.6 mm	2000	9; 1.5 - 9.5; 1	1.04	6.8 mm	6.8 mm	-0.01 mm (-0.2%)
Mean / Deviation	100% Sat	8.0 mm, 1.3 mm	8.4 mm	2000	10; 3.5 - 12.5; 1	0.77	8.8 mm	8.8 mm	0.1 mm (1%)
Mean / Deviation	100% Sat	12.0 mm, 1.3 mm	12.4 mm	2000	9; 7.5 - 15.5; 1	0.48	12.9 mm	12.8 mm	0.2 mm (1%)
Mean / Deviation	100% Sat	2.0 mm, 0.5 mm	2.2 mm	2000	8; 0.25 - 3.75; 0.5	3.56	2.3 mm	2.3 mm	0.0 mm
Mean / Deviation	100% Sat	4.0 mm, 0.5 mm	4.1 mm	2000	8; 2.25 - 5.75; 0.5	1.88	4.3 mm	4.2 mm	0.02 mm (0.5%)
Mean / Deviation	100% Sat	6.0 mm, 0.5 mm	6.1 mm	2000	8; 4.25 - 7.75; 0.5	1.13	6.3 mm	6.3 mm	-0.03 mm (-0.5%)
Mean / Deviation	100% Sat	4.0 mm, 1.3 mm*	4.8 mm	2000	9; 0.5 - 8.5; 1	1.54	5.0 mm	5.0 mm	0.1 mm (2%)
Mean / Deviation	100% Sat	6.0 mm, 2.0 mm*	7.1 mm	1999	9; 0.7 - 11.3; 1.3	0.95	7.4 mm	7.4 mm	0.0 mm
Mean / Deviation	100% Sat	8.0 mm, 2.6 mm*	9.5 mm	2000	9; 1 - 17; 2	0.67	9.9 mm	9.9 mm	0.03 mm (0.3%)
Dissolved O_2	100% Sat	4.0 mm, 1.3 mm	4.8 mm	2000	9; 0.5 - 8.5; 1	1.26	5.0 mm	4.9 mm	0.1 mm (2%)
Dissolved O_2	Min	4.0 mm, 1.3 mm	4.8 mm	2000	9; 0.5 - 8.5; 1	0.79	5.0 mm	4.9 mm	0.1 mm (2%)
Dissolved O_2	Max	4.0 mm, 1.3 mm	4.8 mm	2000	9; 0.5 - 8.5; 1	1.45	5.0 mm	4.9 mm	0.1 mm (2%)
Dissolved O_2	Min	2.0 mm, 0.5 mm	2.2 mm	2000	8; 0.25 - 3.75; 0.5	1.86	2.2 mm	2.3 mm	-0.01 mm (-0.4%)
Dissolved O_2	Max	2.0 mm, 0.5 mm	2.2 mm	2000	8; 0.25 - 3.75; 0.5	3.34	2.3 mm	2.3 mm	-0.01 mm (-0.4%)
Number of bubbles	100% Sat	4.0 mm, 1.3 mm	4.9 mm	200	9; 0.5 - 8.5; 1	1.22	5.1 mm	5.0 mm	0.1 mm (2%)
Number of bubbles	Min	4.0 mm, 1.3 mm	4.9 mm	200	9; 0.5 - 8.5; 1	0.77	5.1 mm	5.0 mm	0.1 mm (2%)
Number of bubbles	Max	4.0 mm, 1.3 mm	4.9 mm	200	9; 0.5 - 8.5; 1	1.40	5.1 mm	5.0 mm	0.1 mm (2%)
Depth: 1.2 m	100% Sat	4.0 mm, 1.3 mm	4.8 mm	2000	9; 0.5 - 8.5; 1	1.26	5.0 mm	4.9 mm	0.1 mm (2%)
Depth: 10 m	100% Sat	4.0 mm, 1.3 mm	4.8 mm	2000	9; 0.5 - 8.5; 1	6.61	5.5 mm	5.4 mm	0.1 mm (2%)
Depth: 25 m	100% Sat	4.0 mm, 1.3 mm	4.8 mm	2000	9; 0.5 - 8.5; 1	10.56	5.8 mm	5.2 mm	0.6 mm (12%)
Depth: 50 m	100% Sat	4.0 mm, 1.3 mm	4.8 mm	2000	9; 0.5 - 8.5; 1	13.82	5.7 mm	3.8 mm	1.9 mm (51%)
Temp: 8°	100% Sat	4.0 mm, 1.3 mm	4.8 mm	2000	9; 0.5 - 8.5; 1	1.37	5.0 mm	4.9 mm	0.1 mm (2%)
Temp: 25°	100% Sat	4.0 mm, 1.3 mm	4.8 mm	2000	9; 0.5 - 8.5; 1	1.56	5.1 mm	5.0 mm	0.1 mm (2%)
Sal: 10 PSU	100% Sat	4.0 mm, 1.3 mm	4.8 mm	2000	9; 0.5 - 8.5; 1	1.47	5.1 mm	5.0 mm	0.1 mm (2%)

Supplementary Table S.6. Comparable fish ponds near the Gerstenteich, June 2021: the stationary feeding sites (F) and sites approx. 55 m away in the direction of the pond centre (M) were investigated using bubble traps over 24 h (or 48 h in the case of low gas volume). Given are the water depth, the ebullition rate and the measured oxygen (O_2) content of the collected bubble gas. Model-derived initial bubble diameter and the bubble diameter at the water surface were determined using mean multiparameter probe profiles (23.6°C, 0.19 psu, 51.0% and 74.6% O_2 saturation for feeding and central sites, respectively) and site-specific dissolved methane (CH_4) and carbon dioxide (CO_2) concentrations. Pure CH_4 bubble were assumed for simulation. The difference between the model-derived bubble diameters at the water surface of both sites is given in mm.

Fish pond	Site	Depth	Ebullition	O_2%	Model-derived diameter		Site	Depth	Ebullition	O_2%	Model-derived diameter		Surface diameter
					initial	surface					initial	surface	difference
		m	ml/m^{2}d	%	mm	mm		m	ml/m^{2}d	%	mm	mm	mm
Inselteich	F	1.5	3465	0.60	6.40	6.63	M	0.7	368	0.82	3.80	3.85	2.78
Thronteich	F	1.3	4504	0.87	4.40	4.52	M	0.6	361	2.23	1.45	1.45	3.07
Kl. Krähenteich	F	1.2	2815	0.67	4.95	5.08	M	0.5	168	4.37	0.80	0.78	4.30
Alter Krähenteich	F	0.9	2201	0.71	3.85	3.92	M	0.6	52	9.43	0.52	0.48	3.44
Brauereiteich	F	1.5	1675	1.12	3.88	3.99	M	1.1	469	1.55	3.05	3.11	0.88
Teich 1	F	1.4	2887	0.79	4.92	5.06	M	1.3	166	1.12	4.89	5.03	0.03
Teich 2	F	2.5	1213	1.55	4.43	4.63	M	1.6	20	4.83	1.58	1.57	3.06
Teich 3	F	1.3	253	4.52	1.11	1.06	M	1.5	94	13.50	0.67	0.60	0.46
Teich 4	F	1.6	4439	1.94	2.36	2.39	M	1.0	22	8.14	0.79	0.75	1.64
Gr. Straßenteich	F	2.0	10213	1.27	4.43	4.60	M	1.2	527	1.53	3.37	3.45	1.15

Supplementary Table S.7. Bubble-sizer results Gerstenteich, Sep 2021: given are the counts of error-free bubble detections and detections with errors, detected and target minutes, ebullition rates and the Sauter mean diameters (SMD) according De Swart et al. (1996) as well as the mean values ± standard deviation (*) or the sum (no marks).

Feeding site	B01						B02					
sampling time	counts		minutes		ebullition	SMD	counts		minutes		ebullition	SMD
7.9.21 11:00	bubbles	errors	detected	target	(ml /m^{2}d)	(mm)	bubbles	errors	detected	target	(ml /m^{2}d)	(mm)
7.9.21 11:40	0	0	0	40			0	0	0	40	-	-
7.9.21 14:45	93	99	9	185	14275	6.5 ± 2.8	0	0	0	185	-	-
7.9.21 17:40	56	7	19	175	5438	7 ± 2.7	0	0	0	175	-	-
7.9.21 20:45	151	32	51	185	5327	7.2 ± 3.2	128	6	102	185	1630	6.6 ± 3.2
7.9.21 23:25	95	33	33	160	5471	7.4 ± 3.6	313	87	98	160	5492	7.7 ± 4
8.9.21 5:45	275	91	80	380	5718	7.1 ± 3.3	272	95	48	380	7339	6.7 ± 3.2
8.9.21 8:25	154	66	29	160	8826	6.7 ± 2.7	77	29	42	160	1115	4.9 ± 2
8.9.21 11:35	144	18	124	190	2788	7.5 ± 2.9	128	95	55	190	4297	9.2 ± 5.7
8.9.21 14:55	212	37	127	200	4370	7.5 ± 2.7	53	49	49	200	1533	6.4 ± 2.2
8.9.21 17:37	191	26	55	162	6530	7 ± 2.8	126	76	87	162	1757	6 ± 1.9
8.9.21 20:20	149	56	31	163	7838	6.8 ± 3	13	14	7	163	1790	5.2 ± 1.1
8.9.21 23:30	190	28	33	190	9726	7 ± 3	159	41	109	190	1726	6.3 ± 2.7
9.9.21 0:30	0	0	0	60	-	-	137	30	50	60	2740	5.7 ± 2.2
sum, mean*	**1710**	**493**	**591**	**2250**	**6937 ± 3138***	**7.1 ± 3.0***	**1406**	**522**	**59**	**184**	**2942 ± 2081***	**6.9 ± 3.3***
Centre of pond	B03						B04					
sampling time	counts		minutes		ebullition	SMD	counts		minutes		ebullition	SMD
7.9.21 10:30	bubbles	errors			(ml /m^{2}d)	(mm)	bubbles	errors			(ml /m^{2}d)	(mm)
7.9.21 12:25	0	0	115		-	-	0	0	115		-	-
7.9.21 18:40	1	1	375		3	5.2	9	4	375		21	4.8 ± 0.6
8.9.21 6:20	15	8	700		19	5.2 ± 1.8	12	26	700		28	7.6 ± 3.9
8.9.21 9:00	0	1	160		-	-	83	53	160		589	6.7 ± 3.3
8.9.21 12:30	0	1	210		-	-	32	9	210		95	4.8 ± 1.7
8.9.21 15:33	8	1	183		44	5 ± 0.4	13	11	183		27	3.9 ± 1.1
8.9.21 23:51	7	6	498		14	4.9 ± 0.3	6	14	498		5	4 ± 1.3
sum, mean*	**31**	**18**			**20 ± 17***	**6.1 ± 2.8***	**155**	**117**			**128 ± 228***	**5.1 ± 1.2***

References

De Swart, J.W.A., van Vliet, R.E., Krishna, R., 1996. Size, structure and dynamics of "large" bubbles in a two-dimensional slurry bubble column. Chem. Eng. Sci. 51, 4619–4629. https://doi.org/10.1016/0009-2509(96)00265-5

Delwiche, K.B., Hemond, H.F., 2017. An enhanced bubble size sensor for long-term ebullition studies. Limnol. Oceanogr. Methods 15, 821–835. https://doi.org/10.1002/lom3.10201

Greinert, J., McGinnis, D.F., 2009. Single bubble dissolution model – The graphical user interface SiBu-GUI. Environ. Model. Softw. 24, 1012–1013. https://doi.org/10.1016/j.envsoft.2008.12.011

Waldemer, C., Koschorreck, M., 2023. Spatial and temporal variability of greenhouse gas ebullition from temperate freshwater fish ponds. Aquaculture.

Table 1. Mean values ± standard deviation of ebullition rates, bubble gas oxygen content, dissolved oxygen saturation, model-derived and Sauter mean (no mark) bubble diameters for bubble traps S01, S02 and S03 and bubble-sizers B01, B02, B03 and B04 at the feeding site and in the open water area of the Gerstenteich.*

Location	Site	Ebullition rate (mL m^{-2} d^{-1})	Bubble oxygen (%)	Dissolved oxygen (%)	Bubble diameter (mm)
Feeding site	S01	38691 ± 9570	0.9 ± 0.3	60.5 ± 23.8	7.2 ± 1.9*
	B01	6937 ± 3138	-	-	7.1 ± 3.0
	B02	2942 ± 2081	-	-	6.9 ± 3.3
Pond center	S02	243 ± 185	4.7 ± 2.2	89.6 ± 18.4	1.6 ± 0.6*
	S03	158 ± 128	6.9 ± 2.8	94.0 ± 21.4	1.1 ± 0.4*
	S02 & S03	198 ± 158	5.9 ± 2.7	91.8 ± 19.7	1.3 ± 0.6*
	B03	20 ± 17	-	-	5.1 ± 1.2
	B04	128 ± 228	-	-	6.1 ± 2.8

Table 2. Published data on bubble size in different freshwater ecosystems. Besides our model, optical bubble sizers and hydroacoustic echosounders were used to determine the mean bubble size. Diurnal variations in bubble size were detected (yes), not observed (no) or not investigated (-), and when the gas composition of the bubble gas was measured, the analyzed gases are reported.

Study site	Method	Bubble diameter (mm)	Diurnal variability	Bubble composition	Reference
Fish pond, Germany	model	Feeding site: 7.2 ± 1.9 Pond center: 1.3 ± 0.6	yes	CH_4, CO_2 & O_2 (all gases)	This study
Wupper reservoir, Germany	optical	6.9	no	-	Schwarz et al. 2023
Upper Mystic Lake, MA, USA	optical	4.6	no	CH_4	Delwiche & Hemond, 2017b
Lake Wohlen reservoir, Switzerland	hydroacoustic	5.9	-	CH_4 estimated from previous work	DelSontro et al., 2015
Lake Kinneret, Israel	hydroacoustic	5.7	-	-	Ostrovsky et al., 2008

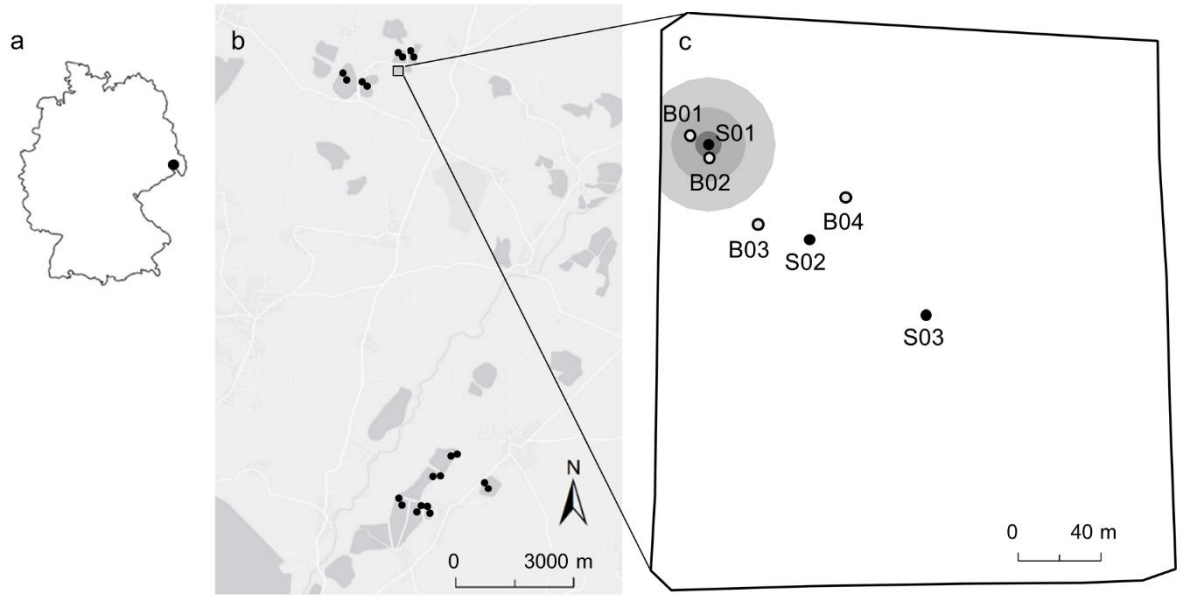

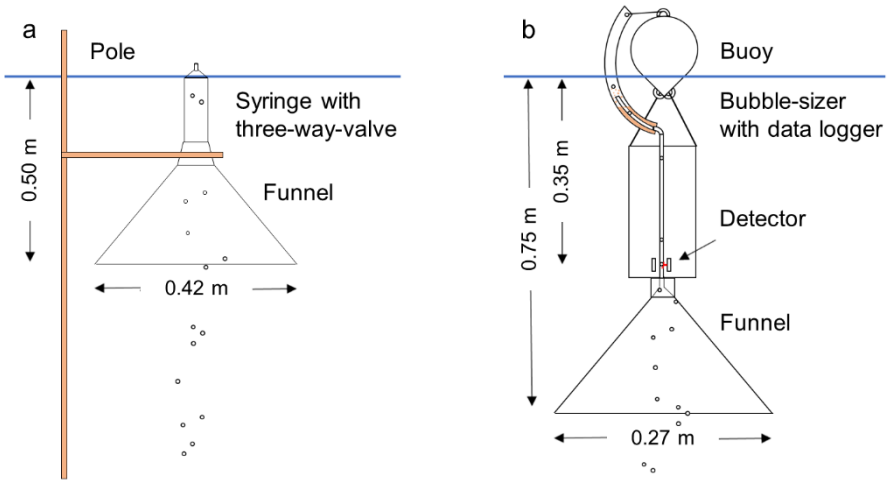

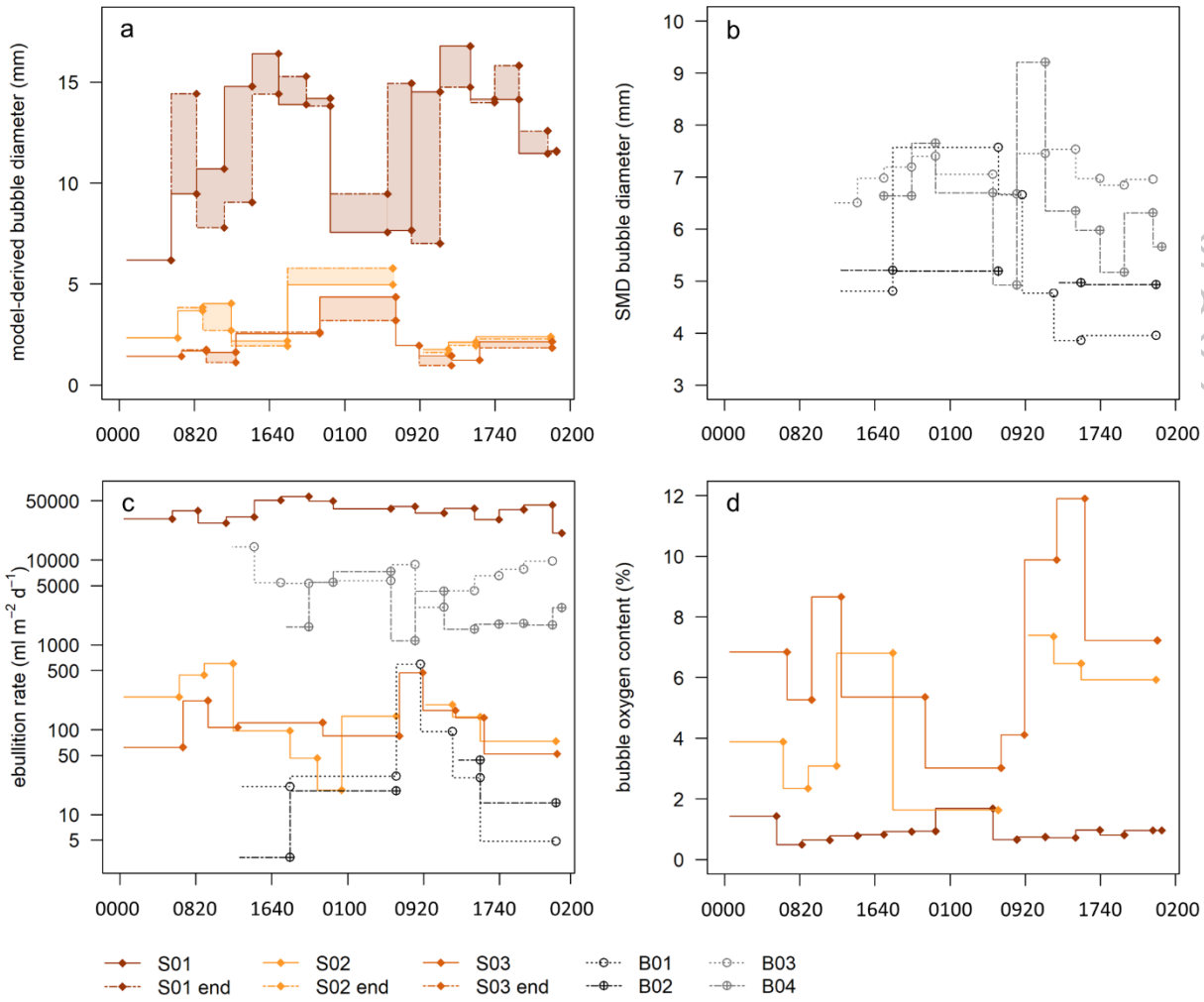
a
model-derived bubble diameter (mm)
0
5
10
15
0000
0820
1640
0100
0920
1740
0200
b
SMD bubble diameter (mm)
3
4
5
6
7
8
9
10
c
ebullition rate (ml m^{-2} d^{-1})
5
10
50
100
500
1000
5000
10000
50000
d
bubble oxygen content (%)
0
2
4
6
8
10
12
S01
S01 end
S02
S02 end
S03
S03 end
B01
B02
B03
B04